Topological properties of minimally doubled fermions in two spacetime dimensions

Stephan Dürr[1,2] and Johannes H. Weber[3]

[1]*Department of Physics, University of Wuppertal, 42119 Wuppertal, Germany*
[2]*Jülich Supercomputing Centre, Forschungszentrum Jülich, 52425 Jülich, Germany*
[3]*Physics Department, Humboldt University of Berlin, D-12489 Berlin, Germany*

The two-dimensional Schwinger model is used to explore how lattice fermion operators perceive the global topological charge $q \in \mathbb{Z}$ of a given background gauge field. We focus on Karsten-Wilczek and Borici-Creutz fermions, which are minimally doubled, and compare them to Wilson, Brillouin, naive, staggered and Adams fermions. For each operator the eigenvalue spectrum in a background with $q \neq 0$ is determined along with the chiralities of the eigenmodes, and the spectral flow of the pertinent Hermitian operator is worked out. We find that Karsten-Wilczek and Borici-Creutz fermions perceive the global topological charge q in the same way as staggered and naive fermions do.

I. INTRODUCTION

How does a given Dirac fermion operator D perceive topology? In lattice gauge theory, this question has been asked persistently over several decades. The answers would be phrased in the language of three "iconic plots": (i) the chiralities $\langle \psi | \gamma_5 | \psi \rangle$ where ψ is an eigenmode of the Dirac operator, (ii) the crossings of the eigenvalues of the Hermitian counterpart operator, and (iii) the fermionic topological charge $q \simeq m \operatorname{tr}(D_m^{-1} \gamma_5)$ versus m.

In this paper we aim to produce such plots for Karsten-Wilczek [1,2] and Borici-Creutz [3,4] fermions. These discretization schemes are in the class of minimally doubled lattice fermion actions, i.e., they yield two species in the continuum limit (precisely the minimum required by the Nielsen-Ninomiya theorem [5–7]) and yet maintain an exact chiral symmetry. Some elementary properties of these formulations like the spectral range and the free field dispersion relations were worked out in Ref. [8]. A slight disadvantage in practical terms is that the remnant chiral symmetry is tasted; this has been discussed in detail in Refs. [9–16].

The compliance of minimally doubled fermions with the Atiyah-Singer index theorem has been discussed in Refs. [17–19]. In our view the topological properties of KW and BC fermions are most transparent if presented alongside "known properties" of more mundane formulations (Wilson, Brillouin, naive, staggered and Adams fermions). In consequence, both the implementation effort and the amount of material to be presented proliferate, and this is why the scope of this paper is limited to two spacetime dimensions ("2D"). We are optimistic that we will follow up with a paper focusing on the situation in four spacetime dimensions ("4D").

We use the quenched Schwinger [20,21] model as a test bed for our calculations, since the set of all $U(1)$ gauge fields on a two-dimensional torus falls into classes labeled by a topological index $q \in \mathbb{Z}$ [22], like in QCD, and the theory can be simulated without topology freezing [23–27]. In 2D fermion matrices tend to be small, and their eigenvalues may be evaluated inexpensively. We apply one step of stout smearing with $\rho = 0.25$ [28] to the "thin link" gauge field U, and evaluate the fermion operators on the resulting "fat link" gauge background V. A preliminary account of this investigation has been given in Ref. [29].

The remainder of this article is organized as follows. The situation for Wilson and Brillouin fermions is reviewed in Sec. II. The details for staggered and Adams fermions are worked out in Sec. III. The relation between the latter two formulations is mirrored by the relation between the naive action without and with an Adams-like taste-splitting term C_{sym}, as shown in Sec. IV. In Sec. V we discuss central-branch fermions and their descendants. Armed with this insight we are in a position to analyze the situation for KW fermions in Sec. VI and for BC fermions in Sec. VII. The lesson learned on species-lifting terms can be applied to KW and BC fermions; in Sec. VIII we demonstrate that this

yields single-taste formulations with additive mass renormalization. Finally, a summary is presented in Sec. IX. Our notation and the Clifford algebra conventions are specified in Appendix A. A side-by-side comparison of all fermionic charge definitions motivated by our investigations is given in Appendix B, and complemented with an analytic argument in Appendix C.

II. WILSON AND BRILLOUIN FERMIONS

The Wilson Dirac operator at vanishing bare mass is defined as [30]

$$D_{\mathrm{W}}(x,y) = \sum_\mu \gamma_\mu \nabla_\mu(x,y) - \frac{ra}{2} \sum_\mu \triangle_\mu(x,y) \qquad (1)$$

and a glimpse at (9) reveals that it differs from the naive Dirac operator by a Hermitian, positive semi-definite term of mass dimension 5. Due to $\triangle_\mu^\dagger = \triangle_\mu$ and $[\triangle_\mu, \gamma_5] = 0$ the Wilson operator is γ_5-Hermitian, i.e., $\gamma_5 D_{\mathrm{W}} \gamma_5 = D_{\mathrm{W}}^\dagger$. An unpleasant feature is that the term $\sum_\mu \triangle_\mu(x,y)$ mixes[1] on interacting gauge backgrounds with the identity. Chiral symmetry is broken, and the bare mass m in the massive operator $D_{\mathrm{N}} + m$ is both additively and multiplicatively renormalized [31]. In the free-field limit the Wilson operator takes a diagonal form in momentum space

$$\begin{aligned} D_{\mathrm{W}}(p) &= \mathrm{i} \sum_\mu \gamma_\mu \frac{1}{a} \sin(ap_\mu) + \frac{r}{a} \sum_\mu \{1 - \cos(ap_\mu)\} \\ &= \mathrm{i} \sum_\mu \gamma_\mu \bar{p}_\mu + \frac{ra}{2} \sum_\mu \hat{p}_\mu^2 \text{ with } \hat{p}_\mu = \frac{2}{a} \sin\left(\frac{ap_\mu}{2}\right), \quad (2) \end{aligned}$$

which again highlights the anti-Hermitian and Hermitian positive semi-definite nature of the two terms, respectively. Specifically for $r = 1$ the $2^{d/2} - 1$ unphysical species do not propagate into any one of the $2d$ on-axis directions [31].

The eigenvalues $\lambda_i \in \mathbb{C}$ of D_{W} on an interacting background with topological charge $q = 1$ are shown in Fig. 1. The result is not far from the free-field case[2] and two depleted areas separate the physical branch at $\mathrm{Re}(\lambda) \simeq 0$ from the two species at $\mathrm{Re}(\lambda) \simeq 2$ and the one at $\mathrm{Re}(\lambda) \simeq 4$. The symmetry about the real axis reflects the pairing property imposed by the γ_5-Hermiticity [31]. Due to the breaking of chiral symmetry the physical branch has a

nonzero renormalized mass [31], and adding a bare mass term $m\delta_{x,y}$ to (1) shifts all eigenvalues by $+m$.

We calculate both the left eigenvector $\langle \psi_i | D_{\mathrm{W}} = \langle \psi_i | \lambda_i$ and the right eigenvector $D_{\mathrm{W}} | \psi_i \rangle = \lambda_i | \psi_i \rangle$ for any (joint) eigenvalue λ_i, with $i = 1, \ldots, 2^{d/2} N_{\mathrm{vol}}$ and $N_{\mathrm{vol}} = N_1 \cdot \ldots \cdot N_d$ the box volume in lattice units. Since D_{W} is non-normal[3] $\langle \psi_i |$ is not related to $|\psi_i\rangle$ by a dagger operation. With the left and the right eigenvectors in hand, one finds $\langle \psi_i | \gamma_5 | \psi_i \rangle$ for each i. The result is plotted as a "needle" above the pertinent $\lambda_i \in \mathbb{C}$ in the right panel. Two needles reach almost down to -1, indicating one species with correct chirality in the physical branch and one in the doubly lifted branch near $\mathrm{Re}(\lambda) \simeq 4$. And two needles reach almost up to $+1$, indicating two species with opposite chirality in the singly-lifted branch near $\mathrm{Re}(\lambda) \simeq 2$.

It is customary to move on to the Hermitian Wilson operator $H_{\mathrm{W}} = \gamma_5(D_{\mathrm{W}} + m)$ [33], and to plot its eigenvalue spectrum (which is in $\mathbb{R}$) as a function of the bare mass m, see Fig. 2. There is one downward crossing near $m = 0$, indicating the fermionic topological charge $q_{\mathrm{W}} = +1$, in line[4] with the topological charge being $q = +1$. However, upon adopting a panoramic view, one sees that there is no net crossing as m tends from $-\infty$ to $+\infty$.

The Brillouin Dirac operator at zero bare mass is defined as [34,35]

$$D_{\mathrm{B}}(x,y) = \sum_\mu \gamma_\mu \nabla_\mu^{\mathrm{iso}}(x,y) - \frac{ra}{2} \triangle^{\mathrm{bri}}(x,y), \qquad (3)$$

where $\nabla_\mu^{\mathrm{iso}}$ denotes a $2 \times 3^{d-1}$-point discretization of the covariant derivative, and $\triangle^{\mathrm{bri}}$ denotes a 3^d-point discretization of the gauged Laplacian. It is conceptually a Wilson-type[5] fermion, albeit with reduced breaking of the hypercubic symmetry.

The eigenvalues $\lambda_i \in \mathbb{C}$ of D_{B} at $m = 0$ on the same background configuration are shown in Fig. 3. The main difference to the Wilson eigenvalue spectrum is that all doublers are located near $\mathrm{Re}(\lambda) \simeq 2$, the physical branch near $\mathrm{Re}(\lambda) \simeq 0$ contains only one species. The additive mass shift is comparable to the Wilson case, and the symmetry about the real axis indicates that D_{B} is γ_5-Hermitian. We compute the left eigenvector $\langle \psi_i |$ and the right eigenvector $|\psi_i\rangle$ for each eigenvalue λ_i, and plot the

---

[1]Another (we think more adequate) view is that the Laplacian consists of two parts, $a^2 \triangle_\mu = 2C_\mu - 2I$, with C_μ given in (A3) and I the identity, and that C_μ (which depends on the gauge field) transforms differently under taste rotations than I (present in $\triangle_\mu$ and the mass term); see footnote 17 for details.

[2]In the free-field case the eigenvalue spectrum of D_{W} follows from γ_μ ($\mu = 1, \ldots, d$) having eigenvalues ± 1. The eigenvalues of D_{W} are inside an ellipse that fits into the rectangle $[0, 2dr] \times [-\sqrt{d}, +\sqrt{d}]$ in d dimensions.

[3]An operator A is normal if $[A, A^\dagger] = 0$. In this case the row-vector $\langle \psi_i |$ is the daggered version of the column vector $|\psi_i\rangle$. In the event A is non-normal, there is no way of obtaining $\langle \psi_i |$ from a single $|\psi_j\rangle$. Here, one needs to combine all column vectors $|\psi_j\rangle$ into a matrix, invert it, and the ith row of the inverse is $\langle \psi_i |$. In the literature the latter statement features as bi-orthogonality condition $\langle \psi_i | \psi_j \rangle = \delta_{ij}$. See Ref. [32] for details.

[4]There is a difference in sign between $d = 2$ and $d = 4$, see discussion in Appendix B.

[5]The Brillouin fermion [34,35] shares this property with the closely related hypercube fermion of Bietenholz et al. [36,37] and the chirally improved fermion of Gattringer et al. [38,39].
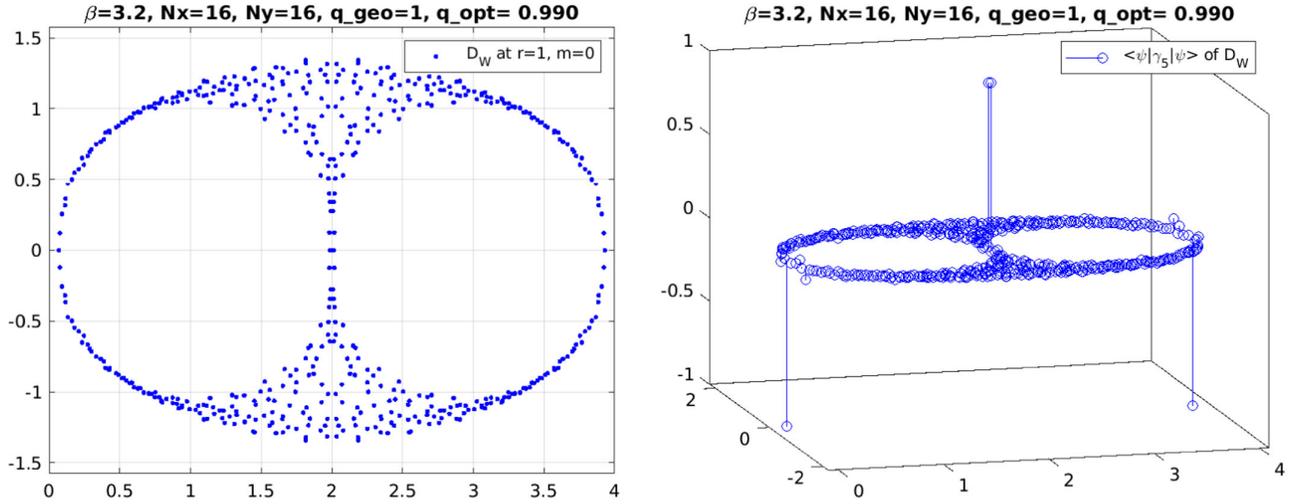
FIG. 1.   Eigenvalues of the Wilson operator on a background with $q = 1$ (left), and "needle plot" of the γ_5-chiralities in the pertinent left-right-eigenvector sandwich (right).
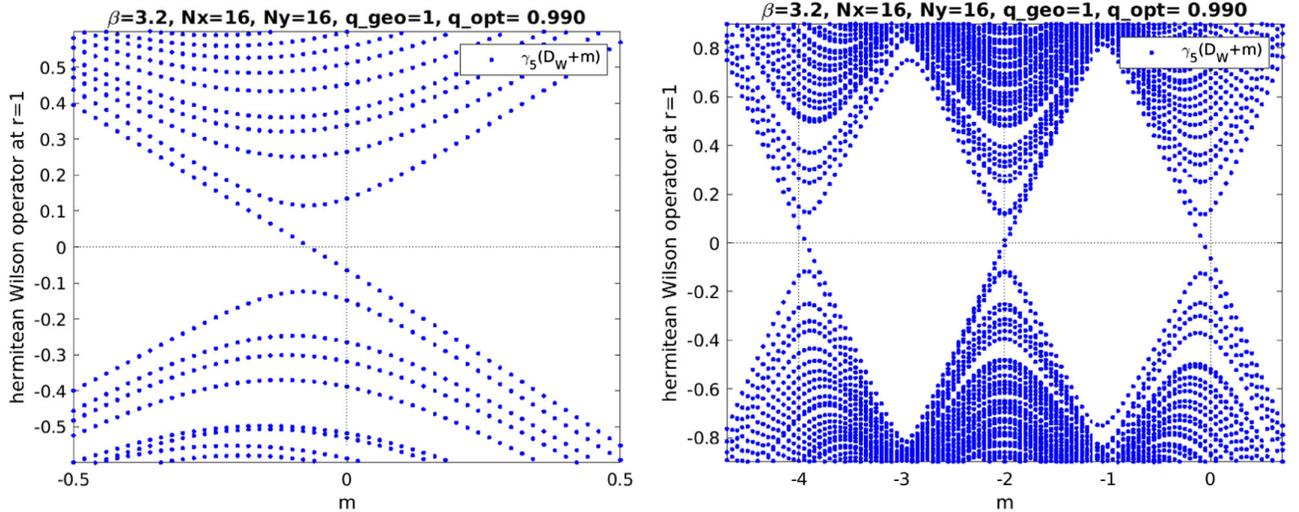

FIG. 2.   Spectral flow of the Wilson operator, i.e., eigenvalues of $\gamma_5(D_W + m)$ versus m. Relevant part near $m = 0$ (left) and panoramic view (right).

chirality $\langle \psi_i | \gamma_5 | \psi_i \rangle$ as a needle at position $\lambda_i \in \mathbb{C}$. The chirality of the would-be zero mode $\lambda \simeq 0.06978$ is almost -1, while the two modes at $1.9972 \pm 0.0012i$ and the one mode at 1.9851 mix[6] heavily.

The eigenvalue flow of the Hermitian Brillouin operator $H_B = \gamma_5(D_B + m)$ is shown in Fig. 4. There is again one eigenvalue crossing near $m = 0$, indicating that the Brillouin operator finds $q_B = +1$, too. In the panoramic view there is no net eigenvalue crossing, though this property is not as easily seen as in the Wilson case.

---

[6]The diagonal elements in this 3×3 block of the chirality matrix read $0.785, 0.785, 1.0$, while the six off-diagonal elements in this block are not close to zero. On the other hand, there is very little mixing between these three modes and the physical mode (out of the six extra off-diagonal elements present in the 4×4 matrix the two largest in magnitude are ± 0.00267).

III. STAGGERED AND ADAMS FERMIONS

The Susskind ("staggered") Dirac operator at vanishing bare mass is defined as [40]

$$D_S(x, y) = \sum_\mu \eta_\mu(x) \nabla_\mu(x, y) \qquad (4)$$

with the Kawamoto-Smit phase factors $\eta_\mu(x) = (-1)^{\sum_{\nu < \mu} x_\nu}$ and $\zeta_\mu(x) = (-1)^{\sum_{\nu > \mu} x_\nu}$ [41]. These are used to define the matrices $\Gamma_\mu(x, y)$, see (A8), which act like γ_μ in spinor space, and the matrices $\Xi_\mu(x, y)$, see (A9), which act like γ_μ in taste[7] space [9–12]. Unlike in the Wilson case,

---

[7]In the latter case the matrix γ_μ is often denoted by ξ_μ, to avoid confusion. In such a situation $\gamma_\alpha \otimes \xi_\beta$ denotes a combined transformation in spinor and taste space, see Refs. [9–12] and Ref. [31].
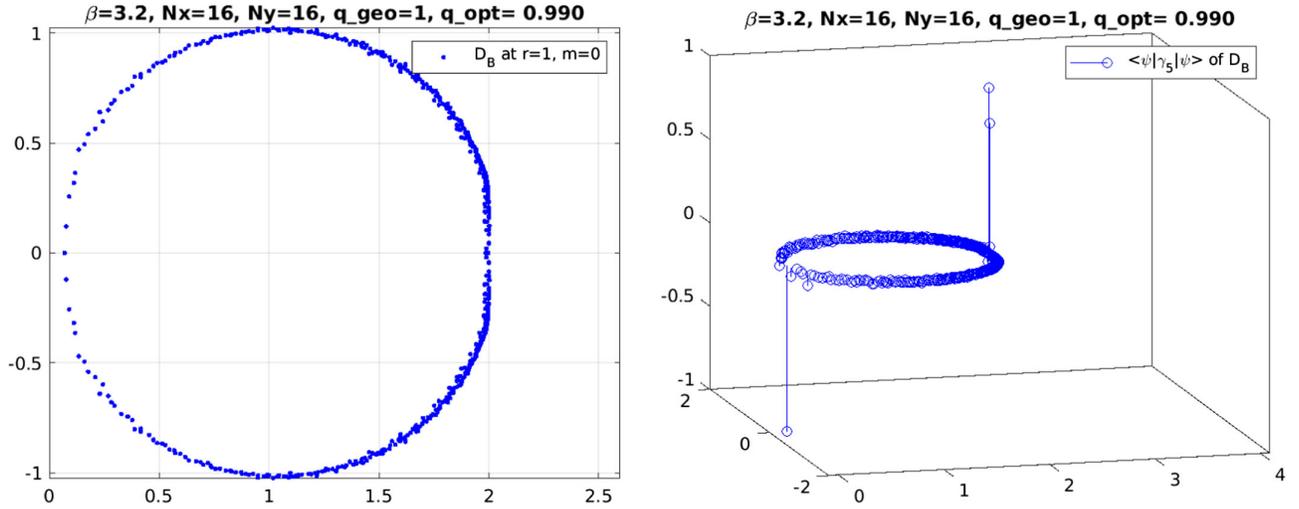
FIG. 3. Eigenvalues of the Brillouin operator on a background with $q = 1$ (left), and "needle plot" of the γ_5-chiralities in the pertinent left-right-eigenvector sandwich (right).
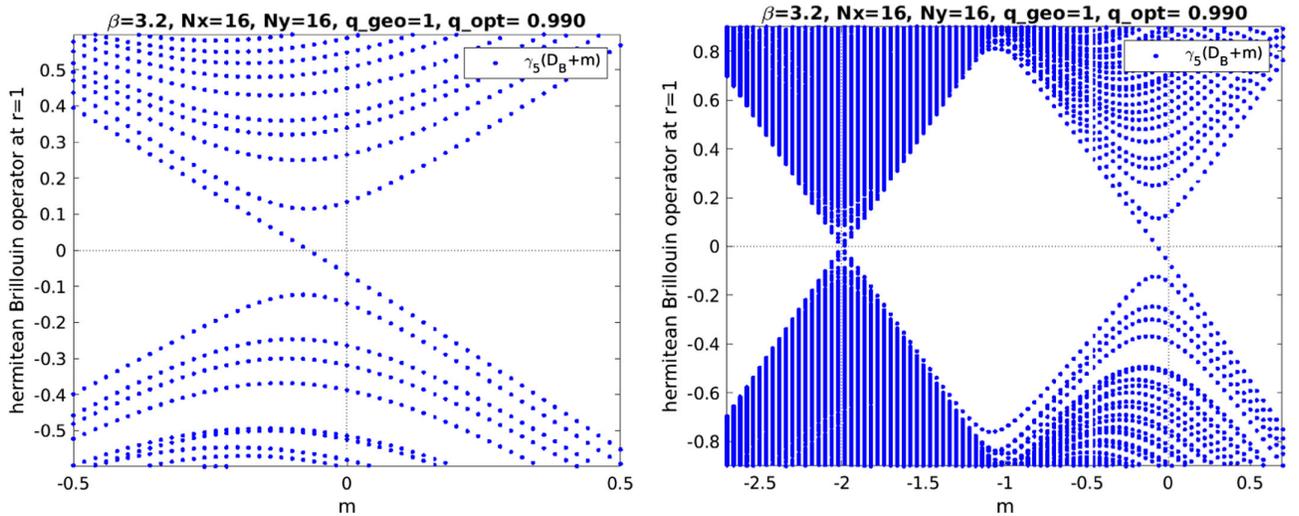

FIG. 4. Spectral flow of the Brillouin operator, i.e., eigenvalues of $\gamma_5(D_B + m)$ versus m. Relevant part near $m = 0$ (left) and panoramic view (right).

these matrices depend on the gauge field U; each Γ_μ or Ξ_μ is a 1-hop operator.

In the following we use the matrix $\Gamma_5(x, y)$ which implements γ_5 in spinor space (up to cutoff effects), and there is a similar matrix $\Xi_5(x, y)$ which implements ξ_5 in taste space (up to cutoff effects). The precise definitions are given in Appendix A. Sometimes a two-index notation is used to refer to the $\gamma \otimes \xi$ decomposition, specifically $\Gamma_{50} \equiv \Gamma_5 \otimes 1$ and $\Gamma_{05} \equiv 1 \otimes \Xi_5$. In this approach Γ_5 and Ξ_5 are extended ultralocal operators (d-hop operators in d dimensions).

Furthermore, there is the 0-hop operator $\epsilon(x, y) = (-1)^{\sum_\mu x_\mu} \delta_{x,y}$, with the representation $\epsilon \doteq \gamma_5 \otimes \xi_5$, and it is sometimes denoted Γ_{55}. Unlike Γ_{50} or Γ_{05}, it does not depend on the gauge background U, but it connects these two matrices by means of the identities

$$\Gamma_{50}(x, y) = \sum_z \epsilon(x, z)\Gamma_{05}(z, y) = \sum_z \Gamma_{05}(x, z)\epsilon(z, y), \quad (5)$$

$$\Gamma_{05}(x, y) = \sum_z \epsilon(x, z)\Gamma_{50}(z, y) = \sum_z \Gamma_{50}(x, z)\epsilon(z, y). \quad (6)$$

In passing we note that all occurrences of U_μ in these formulas should be replaced by the smeared gauge field $V_\mu(x)$, as this greatly reduces the effects of taste symmetry breaking [13–16]. Last but not least, the staggered action (4) is ϵ-Hermitian, i.e., $\epsilon D_S \epsilon = D_S^\dagger$ [31].

The eigenvalue spectrum of D_S on the same gauge configuration as in Sec. II is shown in Fig. 5. The eigenvalues λ_i are purely imaginary, and there is a pairing property $\lambda \leftrightarrow -\lambda$ which reflects the ϵ-Hermiticity. Close inspection reveals that the eigenvalues are twofold nearly degenerate, i.e., each blob in the figure actually represents two nearby eigenvalues. In particular the blob on the real
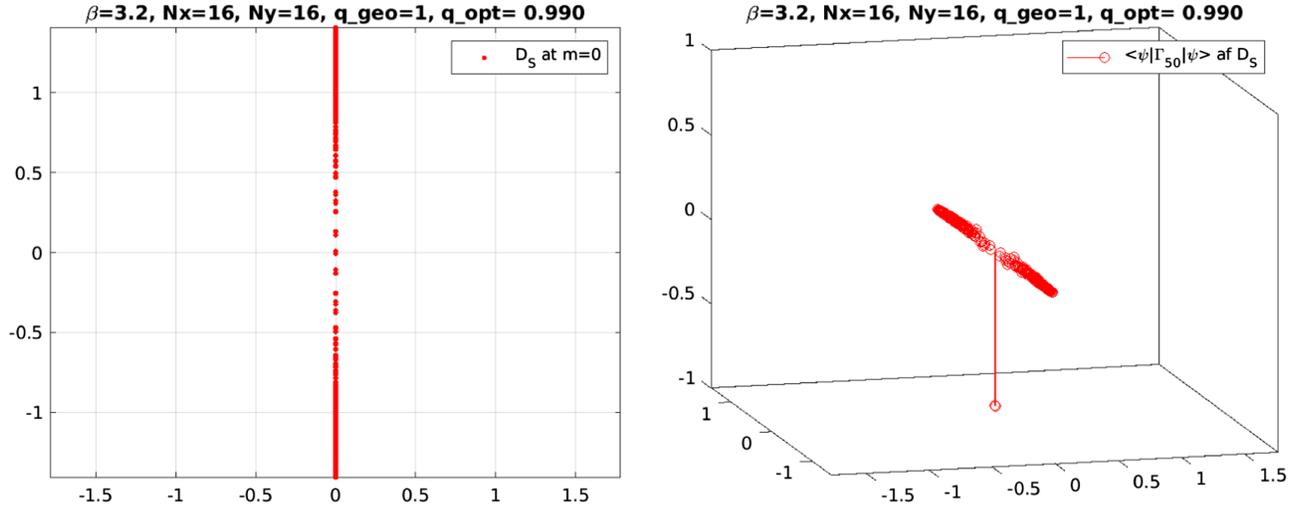
FIG. 5.   Eigenvalues of the staggered operator on a background with $q = 1$ (left), and needle plot of the Γ_{50}-chiralities in the pertinent left-right-eigenvector sandwich (right). The standard ϵ-chiralities or Γ_{55}-chiralities are exactly flat (not shown).
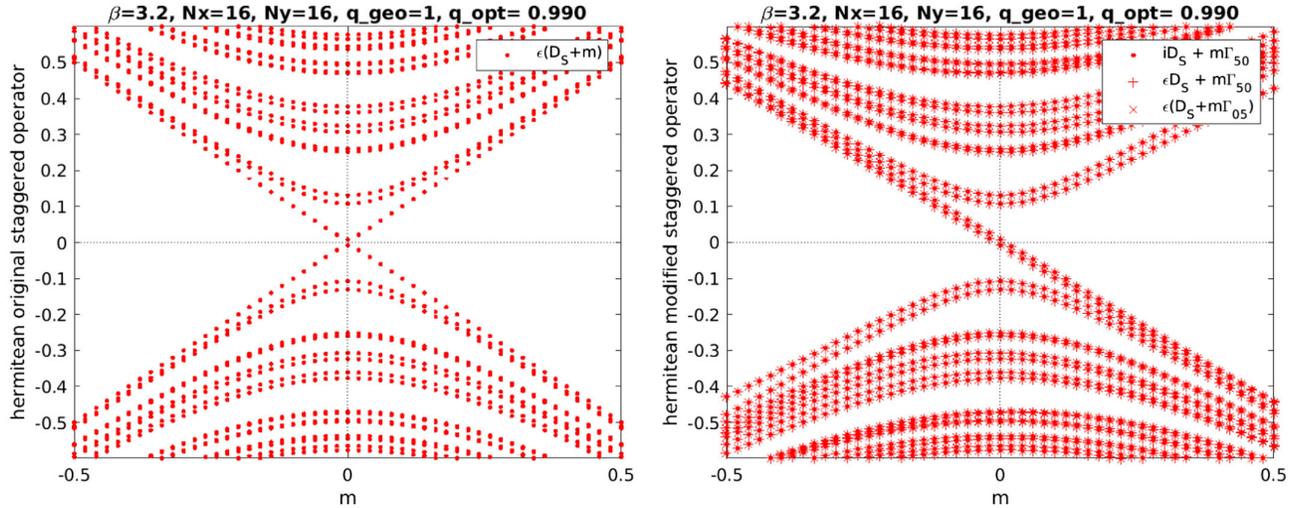

FIG. 6.   Naive spectral flow of the staggered Dirac operator, i.e., eigenvalues of $\epsilon(D_S + m)$ versus m (left), and eigenvalues of $iD_S + m\Gamma_{50}$, $\epsilon D_S + m\Gamma_{50}$, $\epsilon(D_S + m\Gamma_{05})$ versus m (right).

axis represents the two would-be zero eigenvalues[8] expected for topological charge $q = 1$ (in general $2|q|$ for $q \in \mathbb{Z}$). In 4D the near degeneracy is fourfold [42,43].

Like in the previous section, we proceed by calculating all eigenvectors of D_S. Since D_S is normal, it suffices to compute the right eigenvector $|\psi_i\rangle$ for any λ_i, the left eigenvector is just $\langle\psi_i| = (|\psi_i\rangle)^\dagger$. The chirality is defined as the expected value of the chirality operator in the sandwich between $\langle\psi_i|$ and $|\psi_i\rangle$. However, choosing ϵ as the chirality operator is not a good choice, since $\langle\psi_i|\epsilon|\psi_i\rangle = 0$ holds[9] for all modes. Early publications demonstrating (on interacting backgrounds) that one must

use Γ_5 as the chirality operator include [12,44–47]. Choosing Γ_5 as defined in (A4) and representing the chirality $\langle\psi_i|\Gamma_5|\psi_i\rangle$ as a needle over $\lambda_i \in \mathbb{C}$ yields the right panel in Fig. 5. The two would-be zero modes have a chirality close to -1, all other modes have chiralities close to zero. Last but not least, we verified that Ξ_5 is insensitive to topology, i.e., $\langle\psi_i|\Xi_5|\psi_i\rangle \simeq 0$ for all modes. This difference is crucial; it underpins the workings of the staggered flavor interpretation (see Refs. [9–16] and Ref. [31] for a guide to the literature).

The spectral flow of the staggered operator is shown in Fig. 6. A naive analog to $\gamma_5(D_W + m)$ would be $\epsilon(D_S + m)$, but this choice yields no eigenvalue crossing. The more faithful analog is $H_S = \epsilon D_S + m\Gamma_{50}$, since $\Gamma_{50}D_S$ is not Hermitian. Since $\mathrm{spec}(\epsilon D_S) = \mathrm{spec}(iD_S)$, also $iD_S + m\Gamma_{50}$ works fine. Incidentally, this was the first proposal by Adams to generate a staggered spectral

---

[8]The precise values of the two would-be zero eigenvalues are $\lambda \simeq \pm 0.00776i$.
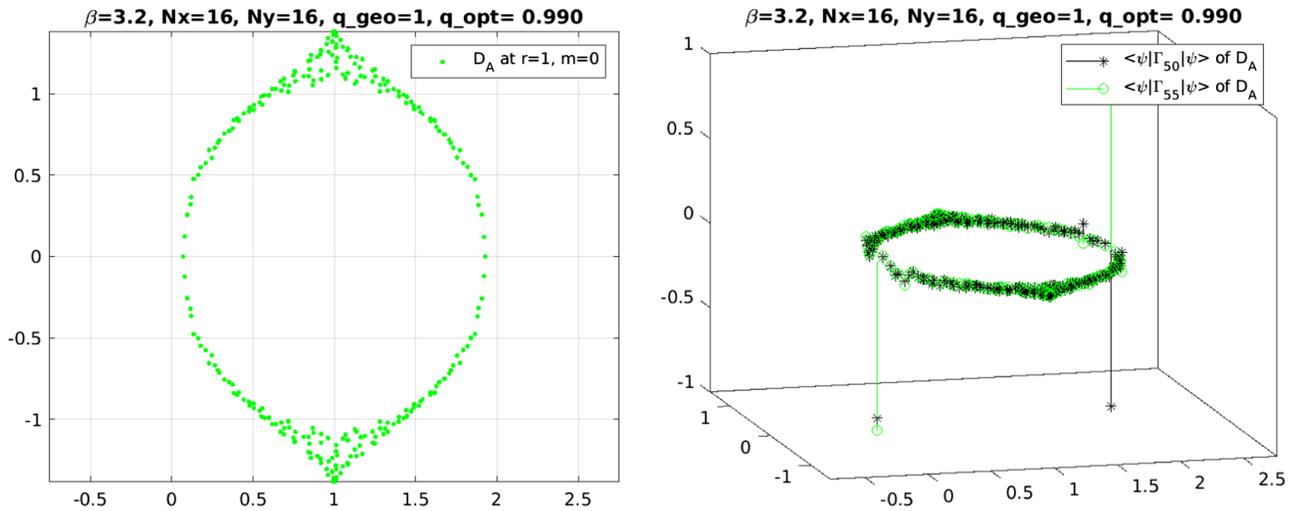[9]This fact occasionally misled people to believe that "staggered fermions are blind to topology."

FIG. 7. Eigenvalues of the Adams operator on a background with $q = 1$ (left), and needle plots of the Γ_{50}-chiralities (black stars) and Γ_{55}-chiralities (open green circles) in the pertinent left-right-eigenvector sandwich (right).
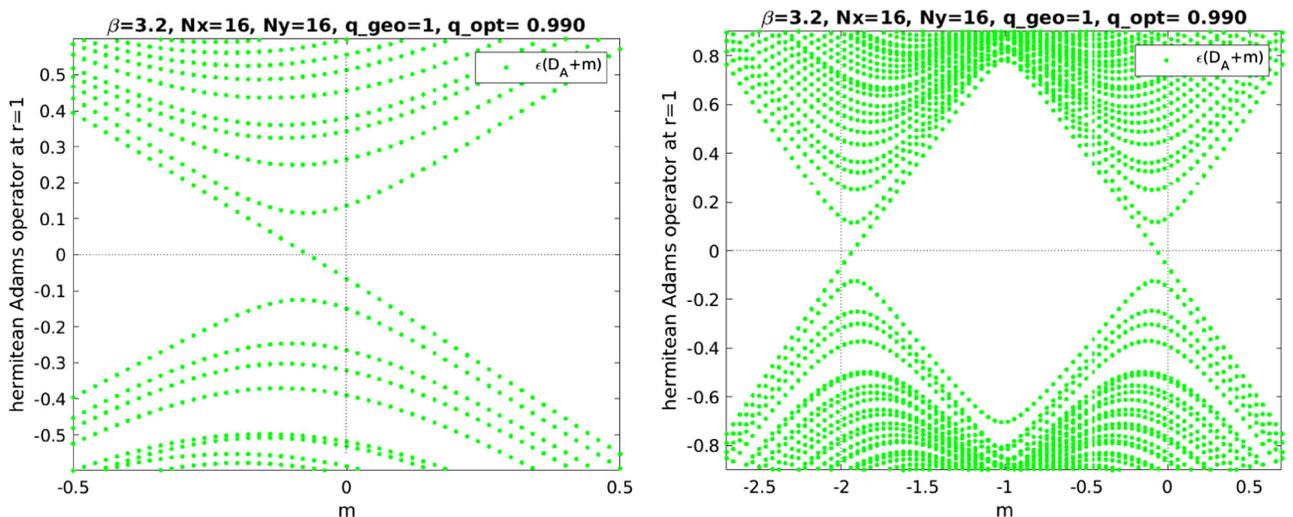

FIG. 8. Spectral flow of the Adams operator, i.e., eigenvalues of $\epsilon(D_A + m)$ versus m. Relevant part near $m = 0$ (left) and panoramic view (right).

flow [48], and it was also used in Ref. [49]. Finally, due to the property (5), (6), the faithful choice is identical to $H_S = \epsilon(D_S + m\Gamma_{05})$ which holds a preview of the Adams operator (see below). These three (non-naive) choices are seen to yield identical results (with two down crossings, as expected for a two-species operator and $q = +1$).

Armed with this insight, we are in a position to esteem the ingenuity of the operator

$$D_A(x, y) = D_S(x, y) + \frac{r}{a}(1 \pm \Gamma_{05}) \qquad (7)$$

proposed by Adams [50]. The choice of sign inside the parentheses depends on the conventions underpinning (A10) and (A11). In practice one will choose it such that

the needle in the physical branch (see below) points in the same direction as in Figs. 1, 3 and 5. In other words, the Adams proposal is to use $\Gamma_{05} = \Xi_5$ to induce a separation between the physical mode[10] and the doubler mode. Like with the other operators, we introduce a Wilson-like deformation parameter r in (7). The Adams operator (7) is ϵ-Hermitian, i.e., $\epsilon D_A \epsilon = D_A^\dagger$.

The eigenvalues of D_A are shown in Fig. 7 (still using the same $q = 1$ background as before). The eigenvalue spectrum is symmetric about the real axis (owing to the

---

[10]In 4D the Adams term $\frac{r}{a}(1 \pm \Gamma_{05})$ causes a splitting between two near-degenerate physical modes and two near-degenerate doublers, see [51–53] for illustrations in the free-field case and the interacting case.

ϵ-Hermiticity), but there is no reflection symmetry about $\mathrm{Re}(z) = 1$. Like in the Wilson-Brillouin case there is a single (exactly real) would-be zero mode in the physical branch (and another one near 2). We compute the left eigenvector $\langle \psi_i |$ and the right eigenvector $|\psi_i\rangle$ for each eigenvalue[11] λ_i and plot the chirality $\langle \psi_i | \epsilon | \psi_i \rangle$ as a needle (with green circle) at position $\lambda_i \in \mathbb{C}$. It is nearly -1 at $\lambda = 0.0706$ (in the physical branch) and nearly $+1$ at $\lambda = 1.9276$ (in the doubler branch). Why is ϵ the correct chirality operator for D_A? The answer was given in the discussion of the (working) spectral flow plot for D_S in Fig. 6. The pluses and crosses give the eigenvalues of

$$\epsilon D_S + m\Gamma_{50} = \epsilon(D_S + m\Gamma_{05}), \qquad (8)$$

where the equality follows from (5), (6). This way Adams managed to have the operator ϵ, which induces the Hermiticity property of D_S, in front, and one recognizes that the term in parentheses is just a shifted version of D_A (with m taking the role of r). Our figure also illustrates what happens if one measures the chirality of D_A with the wrong chirality operator Γ_5 (needles with black stars). This time either branch has a downward-pointing needle, and upon letting $r \to 0$ the situation smoothly turns into the staggered needle plot shown in Fig. 5. Conversely, the Adams choice of chirality, ϵ, is not an option in the staggered case, since upon letting $r \to 0$ the two oppositely oriented needles (green circles) would annihilate in this limit and yield an entirely flat chirality plot (as discussed in the staggered paragraph above).

The spectral flow plot for the Adams operator, i.e., the eigenspectrum of $\epsilon(D_A + m)$ versus m, is shown in Fig. 8. The left panel shows a single down crossing (as expected for an undoubled operator and $q = 1$), the right one clarifies that there is no net crossing. Note that the left panel of Fig. 8 is not identical to the right panel of Fig. 6 (in the former case one sees the effect of additive mass renormalization, like for D_W or D_B, while in the latter case the crossing of the two physical modes is symmetric about $m = 0$). The relationship between these two plots is more subtle—the parameter m in Fig. 6 is a disguised version of r in the Adams operator (7) at $am = -r$, while in Fig. 8 we have $r = 1$ fixed, and the variable m is really a mass.

IV. NAIVE FERMIONS WITHOUT AND WITH SPECIES-LIFTING TERM

The naive Dirac operator at zero bare mass is defined as

$$D_N(x, y) = \sum_\mu \gamma_\mu \nabla_\mu(x, y), \qquad (9)$$

where the anti-Hermitian behavior $\nabla_\mu^\dagger = -\nabla_\mu$ makes the operator γ_5-Hermitian, i.e., $\gamma_5 D_N \gamma_5 = D_N^\dagger$. In the free-field limit this operator assumes a diagonal form in momentum space,

$$D_N(p) = i\sum_\mu \gamma_\mu \frac{1}{a}\sin(ap_\mu) = i\sum_\mu \gamma_\mu \bar{p}_\mu$$

$$\text{with} \quad \bar{p}_\mu = \frac{1}{a}\sin(ap_\mu), \qquad (10)$$

which illustrates the anti-Hermitian nature of the derivative (momentum) term.

Based on the 1-hop operators $C_\mu(x, y)$ given in Appendix A one defines the d-hop operator

$$C_{\mathrm{sym}} = \frac{1}{d!}\sum_{\mathrm{perm}} C_1 C_2 ... C_d \qquad (11)$$

or specifically $C_{\mathrm{sym}} = \frac{1}{2}\{C_1, C_2\}$ in $d = 2$ dimensions, and $C_{\mathrm{sym}} = \frac{1}{24}[C_1 C_2 C_3 C_4 + \mathrm{perm}]$ in $d = 4$ dimensions. Furthermore, there is the operator $\frac{1}{2}(C_1 + C_2)^2 = C_{\mathrm{sym}} + \frac{1}{2}(C_1^2 + C_2^2)$ in 2D. Note that these operators depend on the gauge background (just as Γ_5 and Ξ_5 in Sec. III did).

The eigenvalue spectrum of the naive Dirac operator D_N on our $q = 1$ gauge background is shown in Fig. 9. The dots coincide[12] with the staggered dots in Fig. 5, but there is an additional (exact) twofold[13] degeneracy. The naive operator is "blind to topology" if one uses γ_5 to define chirality, since $\langle \psi_i | \gamma_5 | \psi_i \rangle = 0$ holds for each eigenmode ψ_i of D_N. This situation is reminiscent of choosing ϵ as the chirality operator in the staggered case; this gave $\langle \psi_i | \epsilon | \psi_i \rangle = 0$ for each eigenmode ψ_i of D_S. However, in the staggered case the situation changed by switching to Γ_5 as the chirality operator, and one wonders whether using $C_{\mathrm{sym}} \otimes \gamma_5$ or $\frac{1}{2}(C_1 + C_2)^2 \otimes \gamma_5$ might bring a similar change for the naive Dirac operator. The right panel displays the chirality $\langle \psi_i | C_{\mathrm{sym}} \otimes \gamma_5 | \psi_i \rangle$ as a needle at position $\lambda_i \in \mathbb{C}$ for each i. Hence $C_{\mathrm{sym}} \otimes \gamma_5$ works perfectly as a chirality operator; we find four modes[14] reaching almost down to -1, as expected for a fermion operator which encodes for four continuum species. We also tried $\frac{1}{2}(C_1 + C_2)^2 \otimes \gamma_5$, and the respective needle plot is hard to distinguish from the one in Fig. 9. Still, there is a subtle

---

[11]In doing so we keep in mind that D_A is not normal, $[D_A, D_A^\dagger] \neq 0$, see footnote 3 for details.

[12]The blob on the real axis is at $\lambda \simeq \pm 0.00776i$, cf. footnote 8, and each eigenvalue is twofold degenerate.

[13]In 4D the exact degeneracy is fourfold, but after this degeneracy has been removed the eigenvalue spectrum would again coincide with the staggered eigenvalue spectrum (which in 4D has a fourfold near degeneracy).

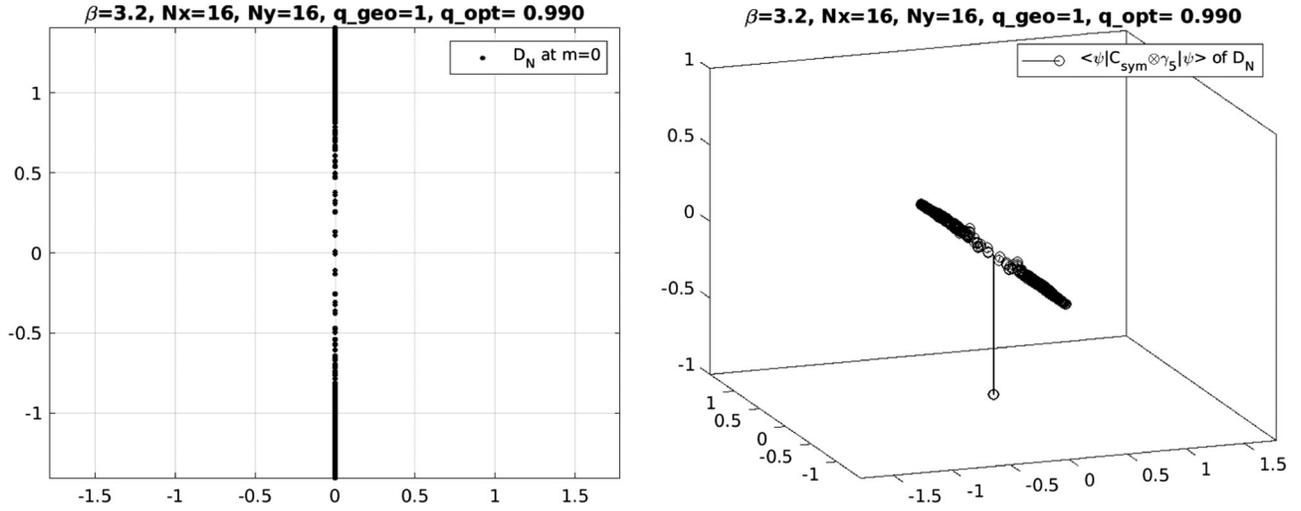[14]In 4D there are 16 needles on a background with $q = \pm 1$; in general 2^d in d spacetime dimensions.

FIG. 9. Eigenvalues of the naive Dirac operator on a background with $q = 1$ (left), and needle plot of the $C_{\text{sym}} \otimes \gamma_5$-chiralities in the pertinent left-right-eigenvector sandwich (right). The $\left[\frac{1}{2}(C_1 + C_2)^2 - 1\right] \otimes \gamma_5$-chiralities look similar, the γ_5-chiralities are zero (not shown).
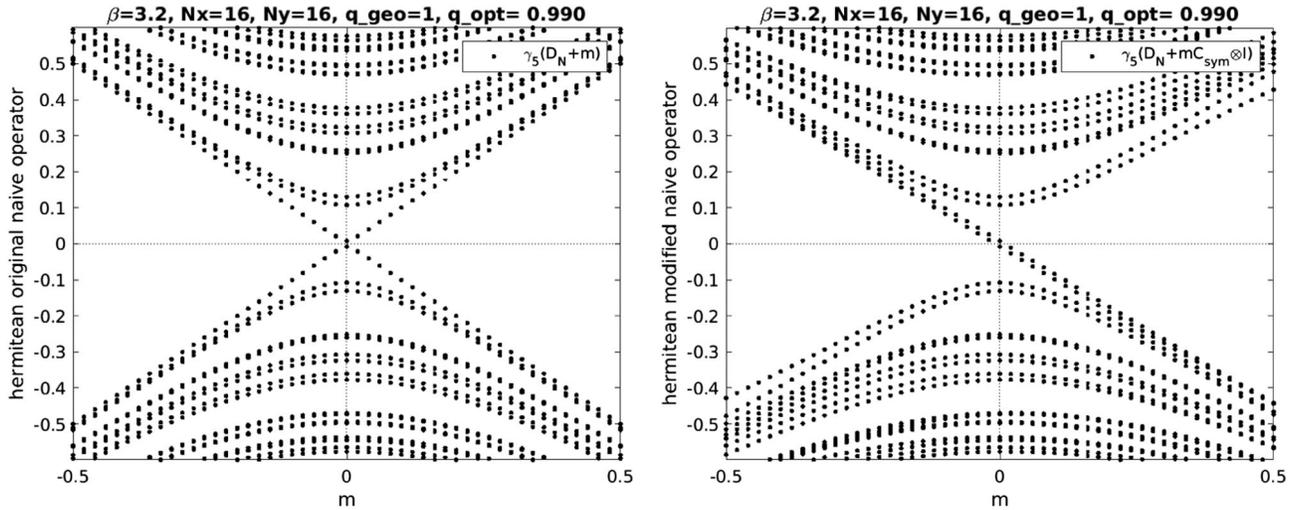

FIG. 10. Spectral flow of the naive Dirac operator, i.e., eigenvalues of $\gamma_5(D_N + m)$ versus m (left), and eigenvalues of $\gamma_5(D_N + mC_{\text{sym}} \otimes 1)$ versus m (right); every point is twofold degenerate.

difference[15] in the sense that the former operator is almost diagonal on the subspace spanned by the would-be zero modes, while the latter one is not. But the chirality operator $\left[\frac{1}{2}(C_1 + C_2)^2 - 1\right] \otimes \gamma_5$ ameliorates the situation again. Its needle plot still looks like that in Fig. 9, while it is again close to diagonal on the subspace spanned by the would-be zero modes.

---

[15]In the subspace of would-be zero modes the chiralities $C_{\text{sym}} \otimes \gamma_5$ and $\frac{1}{2}(C_1 + C_2)^2 \otimes \gamma_5$ take the form

$$
C_{\text{sym}} \otimes \gamma_5 \doteq \begin{pmatrix} -0.9148 & 0.0 & -0.0013 & 0.0 \\ 0.0 & -0.9148 & 0.0 & -0.0013 \\ -0.0013 & 0.0 & -0.9148 & 0.0 \\ 0.0 & -0.0013 & 0.0 & -0.9148 \end{pmatrix}, \frac{1}{2}(C_1 + C_2)^2 \otimes \gamma_5 \doteq \begin{pmatrix} -0.915 & 0.0 & -0.939 & 0.0 \\ 0.0 & -0.915 & 0.0 & 0.936 \\ -0.939 & 0.0 & -0.915 & 0.0 \\ 0.0 & 0.936 & 0.0 & -0.915 \end{pmatrix}
$$

and considering elements $O(10^{-3})$ as zero, the former matrix is diagonal, while the latter one is not. The attentive reader may think of defining new basis vectors, e.g., "(first + third)" or "(second + fourth)" in this subspace, with normalization $1/\sqrt{2}$. The first matrix would be unchanged, while the second one would become close to diagonal. However, this proposal ignores that the first two eigenvectors belong to $\lambda \simeq +0.00776i$, and the latter two to $\lambda \simeq -0.00776i$. Hence, after the proposed rotation, this is no longer an eigenbasis of D_N.
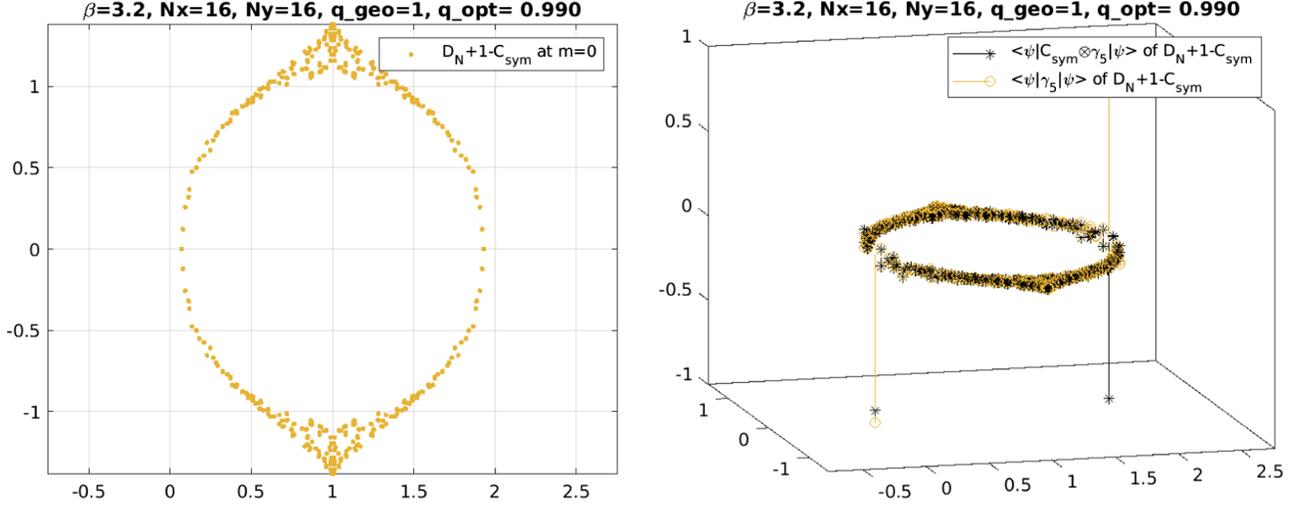
FIG. 11. Eigenvalues of the "Adams-like" Dirac operator $D_N + 1 - C_{sym}$ on a background with $q = 1$ (left), and needle plots of the $C_{sym} \otimes \gamma_5$-chiralities (black stars) and γ_5-chiralities (golden circles) in the pertinent left-right-eigenvector sandwich (right).
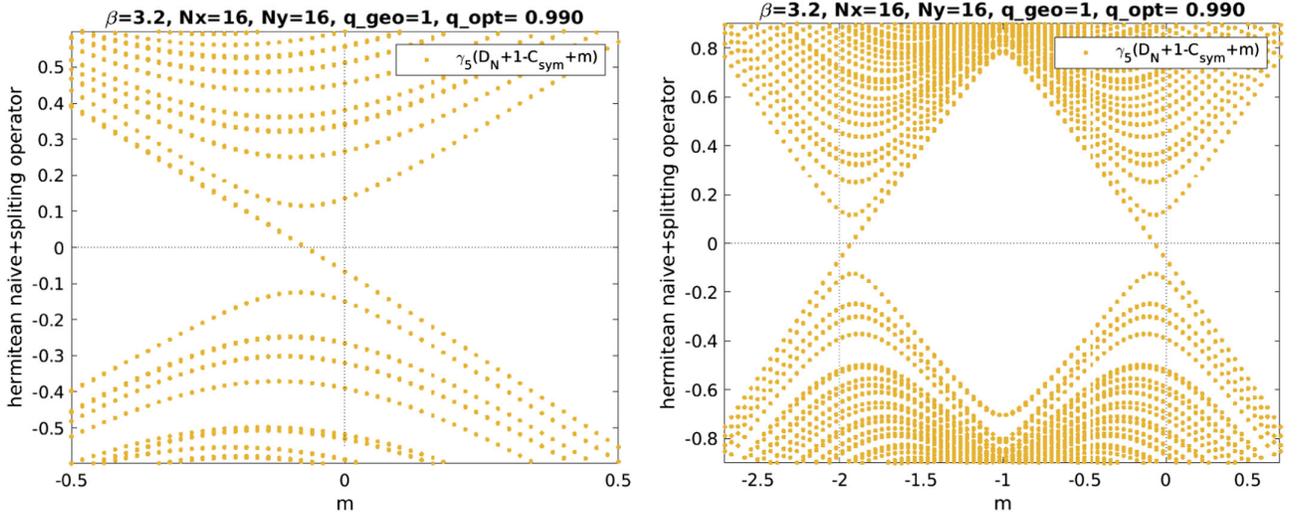

FIG. 12. Spectral flow of the Adams-like Dirac operator, i.e., eigenvalues of $\gamma_5(D_N + 1 - C_{sym} + m)$ versus m. Relevant part near $m = 0$ (left) and panoramic view (right).

The spectral flow plots for the naive action are presented in Fig. 10. Using γ_5 as the chirality operator, D_N shows no crossing; the eigenvalues of $\gamma_5(D_N + m)$ are symmetric under $m \leftrightarrow -m$. This situation is analogous to the staggered case with ϵ as chirality operator. Choosing instead $C_{sym} \otimes \gamma_5$ as chirality operator, the situation changes. In view of the exact twofold degeneracy[16] in the eigenvalues of $\gamma_5(D_N + mC_{sym} \otimes 1)$, there are (in total) four down crossings, as expected for a four-species formulation (in 2D) and $q = 1$. Modulo this degeneracy, the right panel

bears strong similarity with the respective staggered panel, i.e., eigenvalues of $\epsilon(D_S + m\Gamma_{50})$.

Given the similarity between the right panels of Figs. 6 and 10, and bearing in mind the process which led to the construction of D_A in (7), one defines the Adams-like operator

$$D_{like}(x,y) = \sum_\mu \gamma_\mu \nabla_\mu(x,y) + \frac{r}{a}(1 \pm C_{sym})_{x,y}, \quad (12)$$

which realizes a "2 + 2" taste splitting in $d = 2$ dimensions, and an "8 + 8" splitting in $d = 4$ dimensions [19]. In either dimension the splitting is *consistent with chirality*, i.e., the physical modes share one chirality and all doubler modes have opposite chirality. This feature holds true for

---

[16]Choosing instead $[\frac{1}{2}(C_1 + C_2)^2 - 1] \otimes \gamma_5$ as chirality operator, one finds a similar crossing picture, but the eigenvalues of $\gamma_5(D_N + m[\frac{1}{2}(C_1 + C_2)^2 - 1] \otimes 1)$ are twofold near degenerate rather than exactly degenerate.

Adams fermions, provided their chirality is measured with $\Gamma_{55} = \epsilon$. For the operator (12) it holds true in conjunction with the standard γ_5-definition of the chirality.

The eigenvalues $\lambda_i \in \mathbb{C}$ of the Adams-like operator (12) are shown in Fig. 11. The term $1 - C_{\text{sym}}$ separates the two branches nicely, and all eigenvalues are twofold near degenerate. After removing this near degeneracy, the eigenvalue spectrum bears a striking similarity with the one of the Adams operator, see Fig. 7, with a comparable size of the additive mass shift. The would-be zero modes are exactly real, and the eigenvalues associated with non-chiral modes come in complex conjugate pairs, owing to the γ_5-Hermiticity of D_{like}. Unlike in Fig. 7, there is a reflection symmetry about $\text{Re}(z) = 1$. We compute the right eigenvector $|\psi_i\rangle$ and the left eigenvector $\langle\psi_i|$ for each eigenvalue and plot the (correct) chirality $\langle\psi_i|\gamma_5|\psi_i\rangle$ as a needle (golden circle) at position $\lambda_i \in \mathbb{C}$. Two modes in the physical branch reach almost down to -1, and two modes in the doubler branch reach almost up to $+1$. Our figure also illustrates the result of combining the action (12) with the wrong chirality operator $C_{\text{sym}} \otimes \gamma_5$ (needles with black stars). In this case either branch has downward-pointing needles, and upon letting $r \to 0$ the situation smoothly turns into the naive chirality plot shown in Fig. 9. Conversely, the correct choice of chirality, γ_5, is not an option in the naive case, since upon letting $r \to 0$ the two oppositely oriented needles (golden circles) would annihilate in this limit and yield an entirely flat chirality plot (as discussed in the naive paragraph above).

The spectral flow plot of the operator (12), i.e., the eigenvalues of $\gamma_5(D_N + 1 - C_{\text{sym}} + m)$ versus m, is shown in Fig. 12. Each dot represents two nearly degenerate eigenvalues. Considering the situation in the vicinity of $m = 0$ one finds two down crossings, as expected for a two-species formulation and $q = 1$. The right panel shows that there is no net crossing, and the situation is symmetric about $m = -1$ (which holds only approximately in the Adams case).

V. CENTRAL-BRANCH FERMIONS AND DESCENDANTS

The "central-branch" Dirac operator at vanishing bare mass is defined as [54–56]

$$D_{\text{cb}}(x,y) = \sum_\mu \gamma_\mu \nabla_\mu(x,y) + \frac{r}{a}\left[-\frac{a^2}{2}\sum_\mu \triangle_\mu - dI\right]_{x,y}, \quad (13)$$

where I denotes the identity in position space. In the notation of Appendix A the square bracket is $-\sum_\mu C_\mu$, see (A3), and it is evaluated at (x,y) whereupon $I(x,y) = \delta_{x,y}$. In the free-field limit the central branch operator assumes a diagonal form in momentum space

$$D_{\text{cb}}(p) = i\sum_\mu \gamma_\mu \frac{1}{a}\sin(ap_\mu) + \frac{r}{a}\sum_\mu\{0 - \cos(ap_\mu)\}$$

$$= i\sum_\mu \gamma_\mu \bar{p}_\mu + \frac{r}{a}\left[\frac{a^2}{2}\sum_\mu \hat{p}_\mu^2 - d\right], \quad (14)$$

which confirms that it is a shifted version of the Wilson operator (1), (2).

We refrain from showing a plot of the eigenvalues of D_{cb}, since it is just a copy of Fig. 1, but shifted by 2 units to the left. This formulation leads to 2 species in 2D or 6 in 4D. If chirality is measured by the usual γ_5 operator, the physical species *share one chirality*. There is no additive mass renormalization, but one should not be fooled to believe[17] that there is true chiral symmetry. In fact, a close look at Fig. 1 reveals that the eigenvalues in the central branch are slightly "fuzzed" in the horizontal direction, in contradistinction to actions with a remnant chiral symmetry like D_S, D_N, D_{KW} and D_{BC} (cf. Secs. III,IV,VI,VII).

The central-branch-squared Dirac operator (briefly mentioned in Ref. [29]) is defined as

$$D_{\text{cbs}}(x,y) = \sum_\mu \gamma_\mu \nabla_\mu(x,y) + \frac{r}{a}\left[-\frac{a^2}{2}\sum_\mu \triangle_\mu - dI\right]^2_{x,y} \quad (15)$$

and in the free-field limit it assumes a diagonal form in momentum space

$$D_{\text{cbs}}(p) = i\sum_\mu \gamma_\mu \frac{1}{a}\sin(ap_\mu) + \frac{r}{a}\left[\sum_\mu\{0 - \cos(ap_\mu)\}\right]^2$$

$$= i\sum_\mu \gamma_\mu \bar{p}_\mu + \frac{r}{a}\left[\frac{a^2}{2}\sum_\mu \hat{p}_\mu^2 - d\right]^2 \quad (16)$$

which indicates that indeed only the lifting term in (13), (14) is squared. In 2D this operator has two branches with "$2 + 2$" multiplicities, in 4D it has three branches with "$6 + 8 + 2$" multiplicities.

In Fig. 13 the eigenvalue spectrum of D_{cbs} is plotted. In comparison to D_{cb} the recipe (15), (16) squares the

---

[17]It pays to consider the symmetries of the underlying taste structure [57]. The Wilson lifting term is $D_W - D_N = -\frac{a}{2}\sum \triangle_\mu = \frac{1}{a}(-\sum C_\mu + dI)$, where I is the identity. Since γ_5 commutes with both C_μ and I, we have $\{\gamma_5, -\sum C_\mu\} = -2\gamma_5\sum C_\mu$ and $\{\gamma_5, I\} = 2\gamma_5$, so both $\sum C_\mu$ and I break chiral symmetry. Still, there is an important difference between these operators. Let $\tau_{\mu,x} = (-1)^{x_\mu} i\gamma_\mu\gamma_5$ be the generator of the (removable) taste symmetry of naive fermions, and consider a taste rotation $\psi_x \to \tau_{\mu,x}\psi_x$ and $\bar{\psi}_x \to \bar{\psi}_x\tau_{\mu,x}$. Then $D_N(x,y) = \tau_{\mu,x}D_N(x,y)\tau_{\mu,y}$ and $I(x,y) = \tau_{\mu,x}I(x,y)\tau_{\mu,y}$ transform in the same way. But the hopping part of the Wilson term transforms as $C_\mu(x,y) = -\tau_{\mu,x}C_\mu(x,y)\tau_{\mu,y}$ and $C_\nu(x,y) = +\tau_{\mu,x}C_\nu(x,y)\tau_{\mu,y}$ for $\mu \neq \nu$. Hence, I and $\sum C_\mu(x,y)$ in D_W and D_{cb} do not share the full set of symmetries, and renormalize differently. In summary, the central branch term $-\sum C_\mu$ does not mix with the identity, but still breaks chiral symmetry.
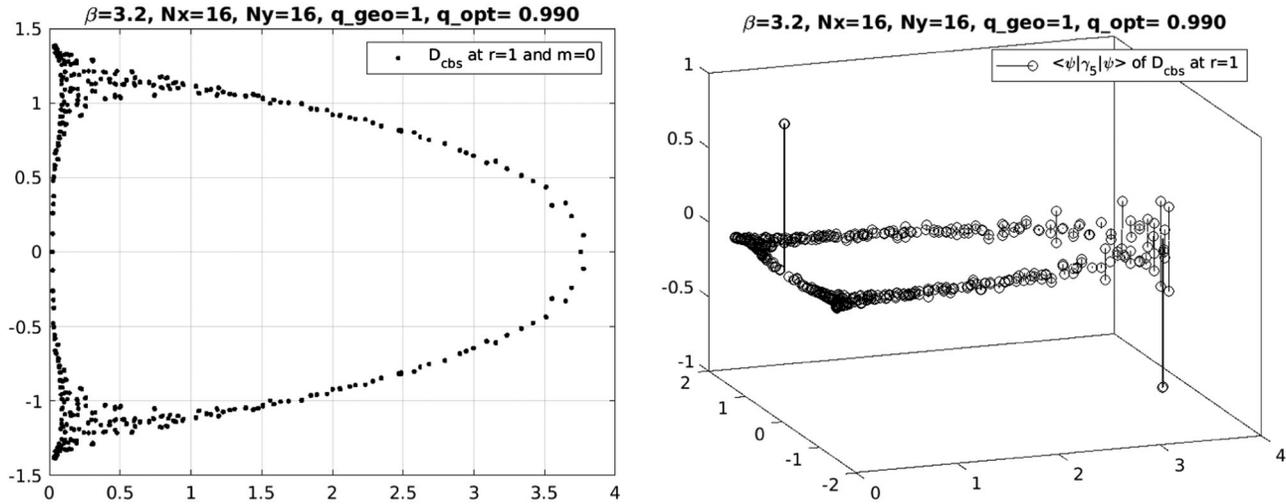
FIG. 13.   Eigenvalues of the "central-branch-squared" Dirac operator at $r = 1$ on a background with $q = 1$ (left), and needle plot of the γ_5-chiralities in the pertinent left-right-eigenvector sandwich (right).
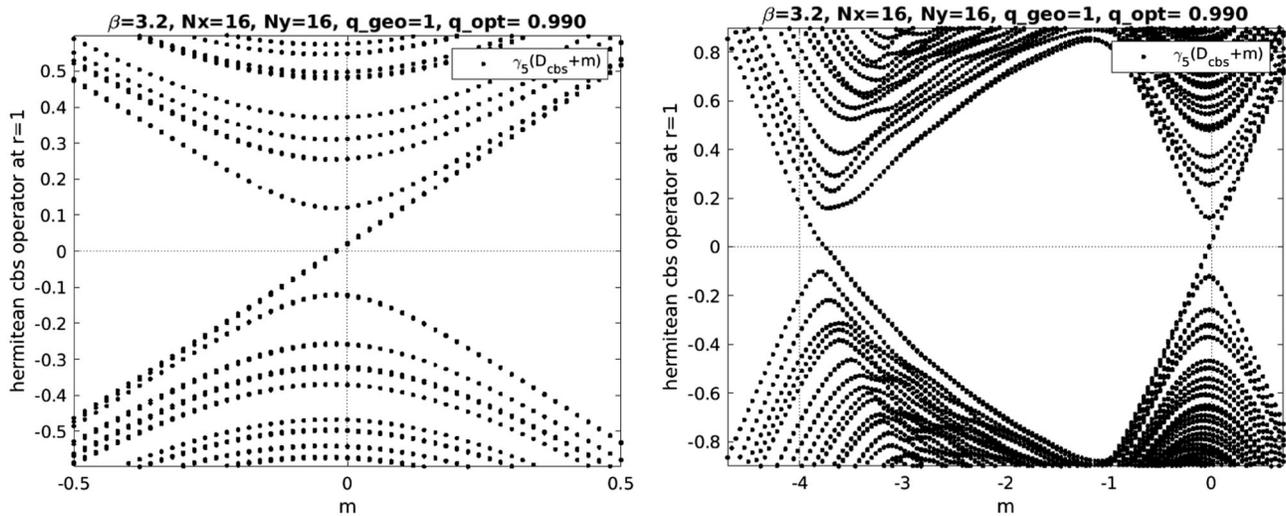

FIG. 14.   Spectral flow of the central-branch-squared Dirac operator at $r = 1$, i.e., eigenvalues of $\gamma_5(D_{\text{cbs}} + m)$ versus m. Relevant part near $m = 0$ (left) and panoramic view (right).

(horizontally acting) Wilson "lifting term" while the (vertically acting) "derivative term" is unaltered. Hence the right (curved) branch in this figure is a superposition of what used to be the leftmost and rightmost branches of the Wilson operator, while the left (near-straight) branch of D_{cbs} is more-or-less identical to the central branch of D_{cb}. Accordingly, the left (near-straight) branch of D_{cbs} hosts two wrong-chirality species, while the right (curved) branch hosts two right-chirality species. A remarkable feature is the unusually small additive mass shift[18] of the near-straight branch. For each eigenvalue λ_i we calculate the left eigenvector $\langle \psi_i |$ and the right eigenvector $| \psi_i \rangle$ of D_{cbs} and determine the chirality

$\langle \psi_i | \gamma_5 | \psi_i \rangle$. The result is displayed as a needle at position $\lambda_i \in \mathbb{C}$. We find two would-be zero modes in the physical branch with chiralities close to $+1$, and two modes in the doubler branch, at $\text{Re}(\lambda) \simeq 4$, with chiralities close to -1. In the physical branch nearby modes tend to have very small chiralities, while in the doubler branch adjacent modes are subject[19] to heavy mixing.

In Fig. 14 the spectral flow of the operator $H_{\text{cbs}} = \gamma_5(D_{\text{cbs}} + m)$ is displayed. There is a twofold (near-degenerate) up crossing at $m \simeq 0$, but there is no net

---

[18]This mass shift is due to the fact that the operators C_μ^2 mix with the identity, while the operators $C_\mu C_\nu$ do not for $\mu \neq \nu$, cf. footnote 17.

[19]This effect is mitigated by using a smaller r; for instance $r = \frac{1}{4}$ reduces the mixing significantly. This is evident from comparing Figs. 13 and 15. The latter figure is *not* a "squeezed" version (by a factor $\frac{1}{4}$) of the former one; the key difference is the amount of "jumping" of the needles near the needle pointing towards -1.
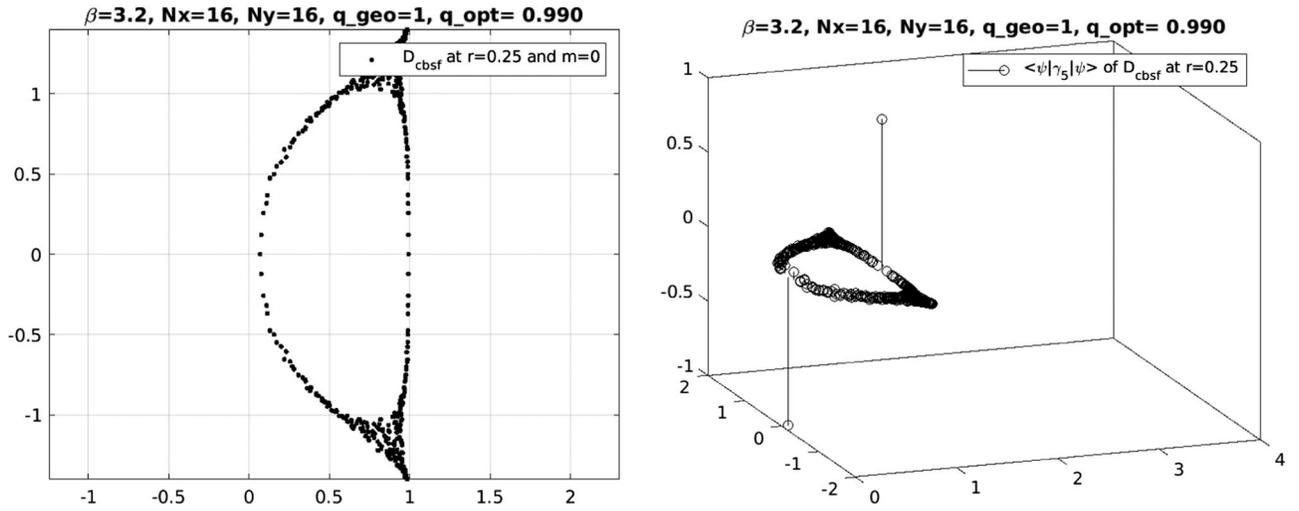
FIG. 15. Eigenvalues of the "central-branch-squared-and-flipped" Dirac operator at $r = \frac{1}{4}$ on a background with $q = 1$ (left), and needle plot of the γ_5-chiralities in the pertinent left-right-eigenvector sandwich (right).
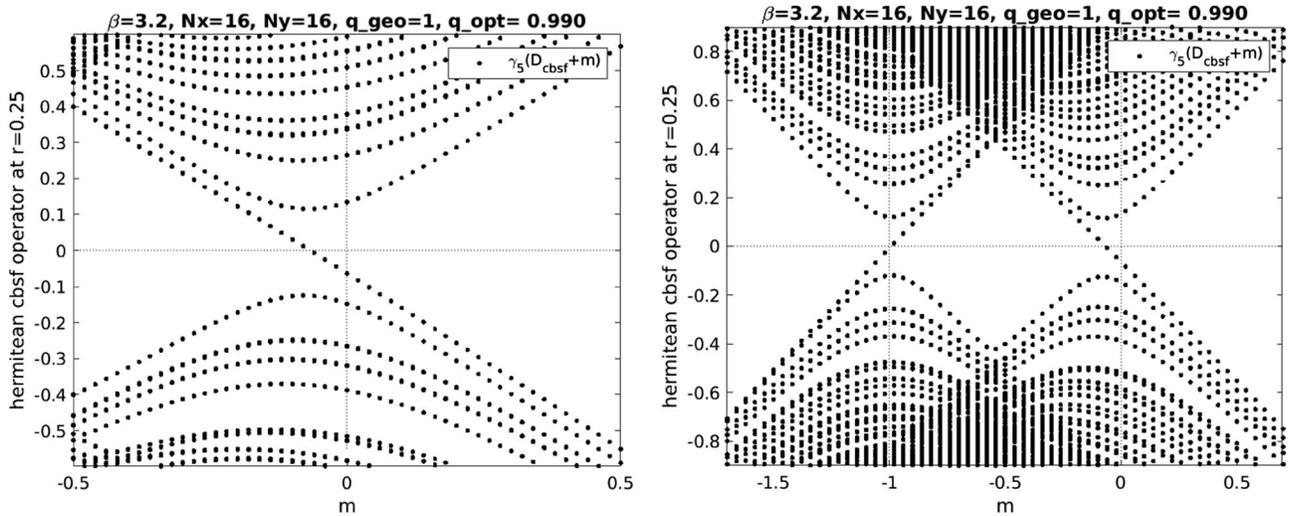

FIG. 16. Spectral flow of the central-branch-squared-and-flipped operator at $r = \frac{1}{4}$, i.e., eigenvalues of $\gamma_5(D_{cbsf} + m)$ versus m. Relevant part near $m = 0$ (left) and panoramic view (right).

crossing on a large scale. The deviation of the up crossing from $m = 0$ is smaller than the deviation of the down crossing from $m = -4r = -4$. This matches, in the eigenvalue plot, the small offset of the physical branch from $\mathrm{Re}(\lambda) = 0$ and the relatively large offset of the doubler branch from $\mathrm{Re}(\lambda) = 4r = 4$.

The central-branch-squared-and-flipped Dirac operator is defined as

$$D_{cbsf}(x, y) = \sum_\mu \gamma_\mu \nabla_\mu(x, y) + \frac{r}{a} d^2 I_{x,y}$$
$$- \frac{r}{a} \left[-\frac{a^2}{2} \sum_\mu \triangle_\mu - dI \right]^2_{x,y}, \qquad (17)$$

where the flipping operation is designed to interchange the physical and the rightmost doubler branches. In 2D this has

no effect on the number of species, but in 4D it trades 6 species for 2.

In Fig. 15 the eigenvalue spectrum of D_{cbsf} at $r = \frac{1}{4}$ is plotted. If we were to stay with $r = 1$ the figure would be a copy of Fig. 13, except for an inversion about $\mathrm{Re}(\lambda) = 2$, and the needle plot would result via the same operation from Fig. 13. In this case we would be confronted with the unpleasant feature that the physical would-be zero modes are in the middle of a region with heavy mixing, as evident from the little spikes nearby. By choosing $r = \frac{1}{4}$ the mixings in the curved (now physical) branch are drastically reduced compared to Fig. 13.

In Fig. 16 the spectral flow of the operator $H_{cbsf} = \gamma_5(D_{cbsf} + m)$ is shown. There is a twofold (near-degenerate) down crossing at $m \simeq 0$, but there is no net crossing on a large scale. The deviation of the down crossing from

$m = 0$ is larger than the deviation of the up crossing from $m = -4r = -1$. This matches, in the eigenvalue plot, the large offset of the physical branch from $\text{Re}(\lambda) = 0$ and the much smaller offset of the doubler branch from $\text{Re}(\lambda) = 4r = 1$.

VI. KARSTEN-WILCZEK FERMIONS

The Karsten-Wilczek proposal is to restrict the Wilson term in (1) to the spatial components

$$D_{\text{KW}}(x, y) = \sum_\mu \gamma_\mu \nabla_\mu(x, y) - \mathrm{i}\frac{ra}{2}\gamma_d \sum_{i=1}^{d-1} \triangle_i(x, y) \qquad (18)$$

with an extra factor $\mathrm{i}\gamma_d$ to make it anti-Hermitian and anticommuting with γ_5 [1,2]. As a result, the Karsten-Wilczek (KW) operator is γ_5-Hermitian, i.e., $\gamma_5 D_{\text{KW}}\gamma_5 = D_{\text{KW}}^\dagger$. In the free-field limit the KW operator assumes a diagonal form in momentum space

$$\begin{aligned} D_{\text{KW}}(p) &= \mathrm{i}\sum_\mu \gamma_\mu \frac{1}{a}\sin(ap_\mu) + \mathrm{i}\frac{r}{a}\gamma_d \sum_{i=1}^{d-1}\{1 - \cos(ap_i)\} \\ &= \mathrm{i}\sum_\mu \gamma_\mu \bar{p}_\mu + \mathrm{i}\frac{ra}{2}\gamma_d \sum_{i=1}^{d-1}\hat{p}_i^2, \end{aligned} \qquad (19)$$

which again indicates that D_{KW} is an anti-Hermitian operator.

This formulation was shown to have 2 species for $r = 1$ in the original works [1,2]. How this number decreases from 2^d, at $r = 0$, to 2, at $r = 1$, has been investigated in Ref. [8]. In $d = 4$ dimensions the number of species is reduced by 2,6,6 at $r = 1/6, 1/4, 1/2$, respectively, so the species chain is $16 \rightarrow 14 \rightarrow 8 \rightarrow 2$. In $d = 2$ dimensions the reduction takes place at $r = 1/2$, so the species chain is $4 \rightarrow 2$. Of course, the number of species is unchanged by a sign flip of r. In Ref. [8] also the free-field (quark-level) dispersion relation of the KW operator is given. In 2D the KW operator (18) takes the simple form (cf. Appendix A)

$$D_{\text{KW}}(x, y) = \sum_\mu \sigma_\mu \nabla_\mu(x, y) - \mathrm{i}\frac{ra}{2}\sigma_2\triangle_1(x, y). \qquad (20)$$

The eigenvalues of the KW operator (20) at $r = 1$ on the same $q = 1$ background as before are displayed in Fig. 17. The spectrum is purely imaginary, like in the staggered or naive case, but it stretches out to ± 3. In the depleted part in the middle, eigenvalues come in near-degenerate pairs (the pair $\lambda = \pm 0.00214\mathrm{i}$ is represented by a single blob on the real axis). We compute the right eigenvector $|\psi_i\rangle$ and the left eigenvector $\langle\psi_i|$ for each eigenvalue $\lambda_i \in \mathbb{C}$. If one were to choose the chirality operator γ_5, the result would be an

entirely flat needle plot. Choosing an appropriate[20] chirality operator like $C_{\text{sym}} \otimes \gamma_5$ the situation is different; for each mode the chirality $\langle\psi_i|C_{\text{sym}} \otimes \gamma_5|\psi_i\rangle$ is plotted as a needle at position $\lambda_i \in \mathbb{C}$. One finds two needles reaching nearly down to -1, as expected for a two-species formulation and $q = 1$.

In Ref. [8] we discuss, for $d = 2$ and $d = 4$, how the KW operator evolves from the naive operator as r increases from 0 to 1. In particular we derive the spectral bound $|\text{Im}(\lambda_{\text{KW}})| \leq \sqrt{2/(1 - r)}$ for $0 \leq r \leq \frac{1}{2}$, and $|\text{Im}(\lambda_{\text{KW}})| \leq 1 + 2r$ for $\frac{1}{2} \leq r$, both valid in the free-field case in 2D. In Fig. 18 the eigenvalue spectrum is shown for a number of r values, along with the spectral bound mentioned. The free-field bound seems to give a rather accurate estimate of the actual spectral range in the interacting case. Defining a would-be zero mode by the (somewhat arbitrary) criterion $|\text{Im}(\lambda_{\text{KW}})| < 1/\sqrt{2N_xN_y}$, the number of would-be zero modes is seen to drop from 4 to 2 in the vicinity of $r = 1/2$, in line with expectations [8].

The spectral flow plot with the inappropriate choice of chirality operator, i.e., the eigenvalues of $\gamma_5(D_{\text{KW}} + m)$ versus m, is shown in Fig. 19. As expected, there is no crossing in the vicinity of $m = 0$. The situation is different with an appropriate chirality operator; the eigenvalues of $\gamma_5(D_{\text{KW}} + mC_{\text{sym}} \otimes 1)$ show a twofold down crossing near $m = 0$. At a superficial level, the latter plot looks similar to the "good" staggered and naive plots in Figs. 6, 10, respectively. Still, there are two notable differences. Compared to the good staggered plot the *intrataste splitting is smaller* (cf. discussion in Sec. VII). Compared to the good naive plot, in addition the (exact) twofold degeneracy is missing.

VII. BORICI-CREUTZ FERMIONS

The basis for Borici-Creutz fermions in d spacetime dimensions is the idempotent operator

$$\Gamma = \frac{1}{\sqrt{d}}\sum_\mu \gamma_\mu \text{ with } \Gamma^2 = \frac{1}{2d}\left\{\sum_\alpha \gamma_\alpha, \sum_\beta \gamma_\beta\right\} = \frac{2d}{2d} = 1 \quad (21)$$

and $\{\Gamma, \gamma_\mu\} = \frac{2}{\sqrt{d}}$ and $\{\Gamma, \gamma_5\} = 0$. This suggests to define the dual gamma matrices

$$\gamma'_\mu = \Gamma\gamma_\mu\Gamma = \left(\frac{2}{\sqrt{d}} - \gamma_\mu\Gamma\right)\Gamma = \frac{2}{\sqrt{d}}\Gamma - \gamma_\mu, \quad (22)$$

---

[20]The KW operator has two zeros in the Brillouin zone, with opposite chiralities due to the Nielsen-Ninomiya theorem [5–7]. In the free field case they are located at $ap_d = 0, \pi$ (with $ap_i = 0$ for $i = 1, ..., d - 1$), and encode the same chiralities as for naive fermions [8]. Therefore, the same chirality operators can be employed for KW and naive fermions. We found good results with both $C_{\text{sym}} \otimes \gamma_5$ and $[\frac{1}{2}(C_1 + C_2)^2 - 1] \otimes \gamma_5$ at $r = 1$.
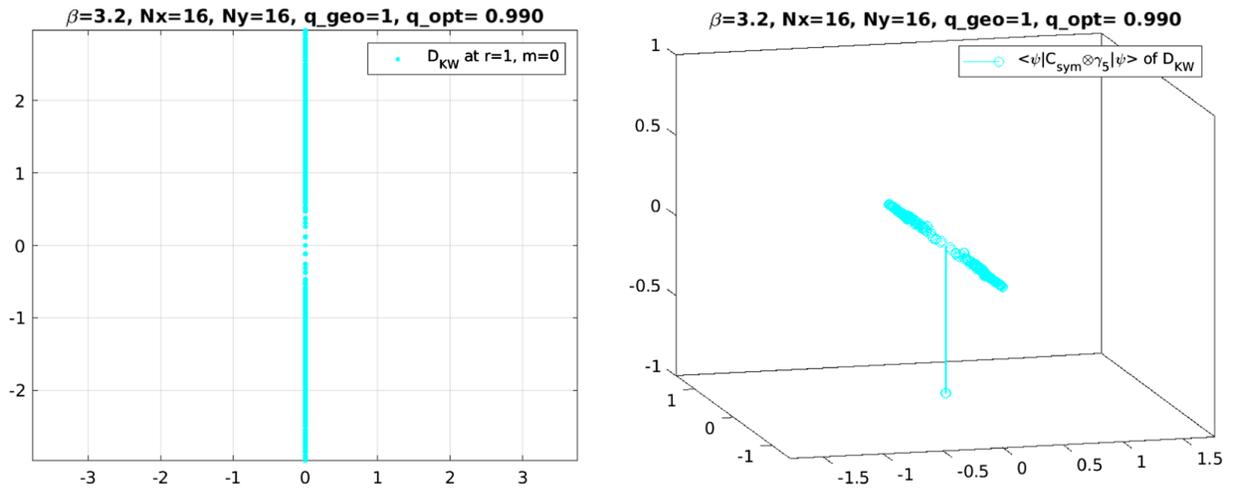
FIG. 17.   Eigenvalues of the KW Dirac operator on a background with $q = 1$ (left), and needle plot of the $C_{\mathrm{sym}} \otimes \gamma_5$-chiralities in the pertinent left-right-eigenvector sandwich (right). The standard γ_5-chiralities are exactly flat (not shown).
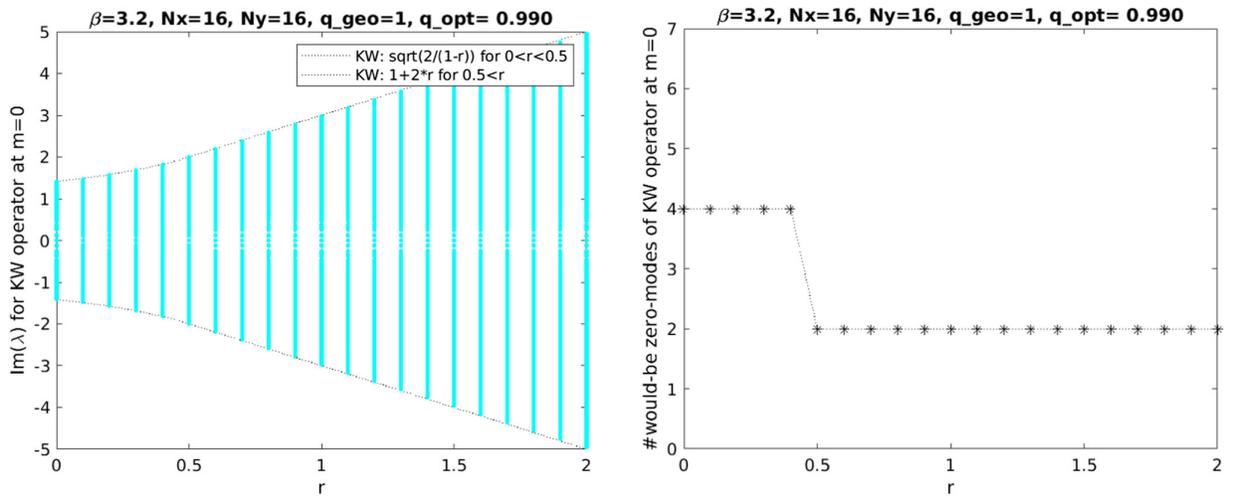

FIG. 18.   Eigenvalues of the KW Dirac operator on an interacting background as a function of the species-lifting parameter r (left), and number of would-be zero modes versus r (right).
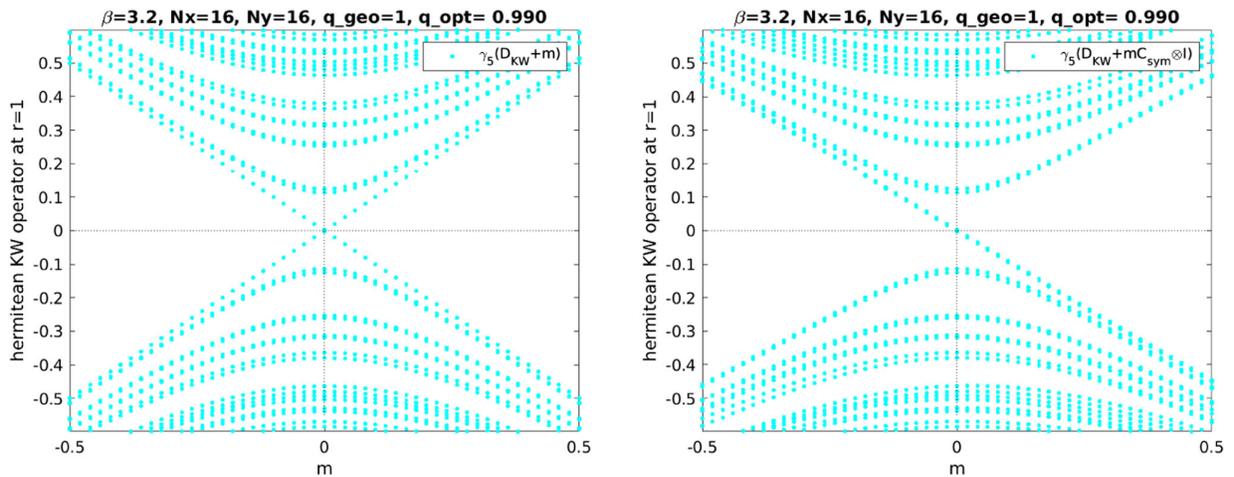

FIG. 19.   Spectral flow of the KW Dirac operator, i.e., eigenvalues of $\gamma_5(D_{\mathrm{KW}} + m)$ versus m (left), and eigenvalues of $\gamma_5(D_{\mathrm{KW}} + mC_{\mathrm{sym}} \otimes 1)$ versus m (right).

which are Hermitian and satisfy the Dirac-Clifford algebra, since (22) implies $\{\gamma'_\mu, \gamma'_\nu\} = 2\delta_{\mu\nu}$ and $\{\Gamma, \gamma'_\mu\} = \frac{2}{\sqrt{d}}$. Furthermore, one finds $\{\gamma_\mu, \gamma'_\nu\} = \frac{4}{d} - 2\delta_{\mu\nu} = \{\gamma'_\mu, \gamma_\nu\}$.

The Borici-Creutz (BC) proposal is to dress the Wilson term in (1) with i times (22),

$$D_{\mathrm{BC}}(x, y) = \sum_\mu \gamma_\mu \nabla_\mu(x, y) - \mathrm{i}\frac{ra}{2}\sum_\mu \gamma'_\mu \triangle_\mu(x, y), \qquad (23)$$

where our second term differs in sign from the original proposal [3,4]. Note that the second term is anti-Hermitian and anticommutes with γ_5, since

$$\gamma'_\mu \gamma_5 = \Gamma\gamma_\mu \Gamma\gamma_5 = -\Gamma\gamma_\mu \gamma_5 \Gamma$$
$$= \Gamma\gamma_5 \gamma_\mu \Gamma = -\gamma_5 \Gamma\gamma_\mu \Gamma = -\gamma_5 \gamma'_\mu \qquad (24)$$

and this renders the BC operator γ_5-Hermitian, i.e., $\gamma_5 D_{\mathrm{BC}} \gamma_5 = D_{\mathrm{BC}}^\dagger$. In the free-field limit the BC operator assumes a diagonal form in momentum space

$$D_{\mathrm{BC}}(p) = \mathrm{i}\sum_\mu \gamma_\mu \bar{p}_\mu + \mathrm{i}\frac{r}{a}\sum_\mu \gamma'_\mu \{1 - \cos(ap_\mu)\}$$
$$= \mathrm{i}\sum_\mu \gamma_\mu \bar{p}_\mu + \mathrm{i}\frac{ra}{2}\sum_\mu \gamma'_\mu \hat{p}_\mu^2 \qquad (25)$$

in which the bracket $\{1 - \cos(ap_\mu)\}$ may be split and the sum over γ'_μ performed by means of

$$\sum_\mu \gamma'_\mu = 2\sqrt{d}\Gamma - \sum_\mu \gamma_\mu$$
$$= 2\sqrt{d}\Gamma - \sqrt{d}\Gamma = \sqrt{d}\Gamma. \qquad (26)$$

The free-field form (25) highlights the invariance under any permutation of the d axes.

This formulation was shown to have 2 species for $r = 1$ in the original works [3,4]. How this number decreases from 2^d, at $r = 0$, to 2, at $r = 1$, has been investigated in Ref. [8]. In 4D one starts with 16 species, and this number decreases by 6 at $r = 1/\sqrt{3}$, and by 8 at $r = 1/\sqrt{2}$; so the species chain is $16 \rightarrow 10 \rightarrow 2$. In 2D one starts with 4 species, and this number decreases by 2 at $r = 1/\sqrt{3}$; so the species chain is $4 \rightarrow 2$. A sign flip in r affects the location of the doubler mode in the Brillouin zone (cf. footnote 21) but not the number of physical modes. For the free-field (quark-level) dispersion relation see Ref. [8]. In 2D the BC operator (23) takes the simple form (cf. Appendix A)

$$D_{\mathrm{BC}}(x, y) = \sum_\mu \sigma_\mu \nabla_\mu(x, y) - \mathrm{i}\frac{ra}{2}\sigma_2 \triangle_1(x, y)$$
$$- \mathrm{i}\frac{ra}{2}\sigma_1 \triangle_2(x, y) \qquad (27)$$

and comparing this to (20) shows that the BC operator is not a symmetrized form of the KW operator; it has an extra term. This is why, in Eqs. (23), (25), the sign of the

r-dependent term differs from the literature. With our convention the joint terms in Eqs. (20), (27) have like sign.

The eigenvalues of the BC operator (27) at $r = 1$ on the same $q = 1$ background as before are displayed in Fig. 20. The spectrum is purely imaginary (as for the previously discussed chiral actions), but this time it stretches out to $\pm(2 + \sqrt{2})$. In the depleted part in the middle, eigenvalues come in near-degenerate pairs (the pair $\lambda = \pm 0.00854\mathrm{i}$ is represented by a single blob on the real axis). We compute the right eigenvector $|\psi_i\rangle$ and the left eigenvector $\langle\psi_i|$ for each eigenvalue $\lambda_i \in \mathbb{C}$. With γ_5 as chirality operator, one obtains $\langle\psi_i|\gamma_5|\psi_i\rangle = 0$ for all modes ψ_i. Choosing $[2C_{\mathrm{sym}} - 1] \otimes \gamma_5$ as chirality operator[21] the situation is different; for each mode the chirality $\langle\psi_i|[2C_{\mathrm{sym}} - 1] \otimes \gamma_5|\psi_i\rangle$ is plotted as a needle at position $\lambda_i \in \mathbb{C}$. One finds two needles reaching nearly down to -1, as expected for a two-species formulation and $q = 1$.

In Ref. [8] we discuss how the BC operator evolves from the naive operator as r increases from 0 to 1. In particular we derive the spectral bound $|\mathrm{Im}(\lambda_{\mathrm{BC}})| \leq \sqrt{d}(r + \sqrt{1 + r^2})$ for $0 \leq r$, valid in the free-field case in d dimensions. In Fig. 21 the eigenvalue spectrum is shown for a number of r values, along with the spectral bound mentioned (for $d = 2$). The free-field bound seems to give a rather accurate estimate of the actual spectral range in the interacting case. Defining a would be zero mode by the same criterion as in Sec. VI, their number is seen to evolve from 4 to 2 in the vicinity of $r = 1/\sqrt{3}$, in line with expectations [8].

As for naive or KW fermions, γ_5 is an inappropriate choice of the chirality operator; the eigenvalues of $\gamma_5(D_{\mathrm{BC}} + m)$ versus m show no crossing, see Fig. 22. With the appropriate chirality operator the situation is different; $\gamma_5(D_{\mathrm{BC}} + m[2C_{\mathrm{sym}} - 1] \otimes 1)$ reveals the expected two-fold eigenvalue down crossing near $m = 0$. At a superficial level, the latter plot looks similar to the good staggered plot in Fig. 6, the good naive plot in Fig. 10, and the good KW plot in Fig. 19 (modulo degeneracies).

Upon comparing these four plots more diligently, one notices that (apart from the extra twofold exact degeneracy in the naive case) these plots differ by the *size of the taste breaking*. Taking the splitting between the two down crossings in Figs. 6 and 10 as a basis, the splitting in the

---

[21]As for KW fermions, the two surviving zero modes of BC fermions must encode opposite γ_5 chiralities, due to the Nielsen-Ninomiya theorem [5–7]. An extended splitting operator separates these cleanly if it assumes opposite (nonzero) real values at these two positions. The two zero modes of BC fermions surviving in the free theory are located at $ap_\mu = 0$ and $ap_\mu = \kappa(r)$, with $\kappa(r) \equiv -2\arctan(1/r)$ for all d components of ap [8]. For the canonical value $r = 1$, the second mode is thus at $\kappa(1) = -\pi/2$. While the operator $C_{\mathrm{sym}}(k)$ assumes the value 1 at $ap_\mu = 0$, it yields 0 at $ap_\mu = -\pi/2$. A deformation of $C_{\mathrm{sym}}(k)$ that realizes the desired sign change is $(1 + A(r))C_{\mathrm{sym}} - A(r)$ with $A(r) = [2 + \cos^2(\kappa(r))]/[2 - \cos^2(\kappa(r))]$; this yields $A(1) = 1$. We found good chirality results with both $[2C_{\mathrm{sym}} - 1] \otimes \gamma_5$ and $[\frac{1}{2}(C_1 + C_2)^2 - 1] \otimes \gamma_5$ at $r = 1$.
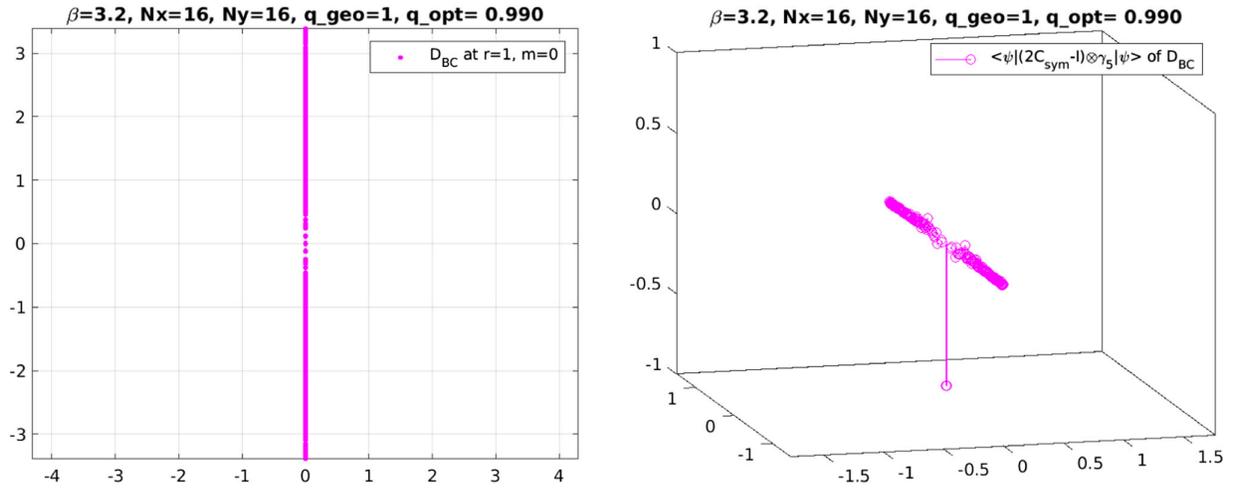
FIG. 20. Eigenvalues of the BC Dirac operator on a background with $q = 1$ (left), and needle plot of the $[2C_{\text{sym}} - 1] \otimes \gamma_5$-chiralities in the pertinent left-right-eigenvector sandwich (right). The standard γ_5-chiralities are exactly flat (not shown).
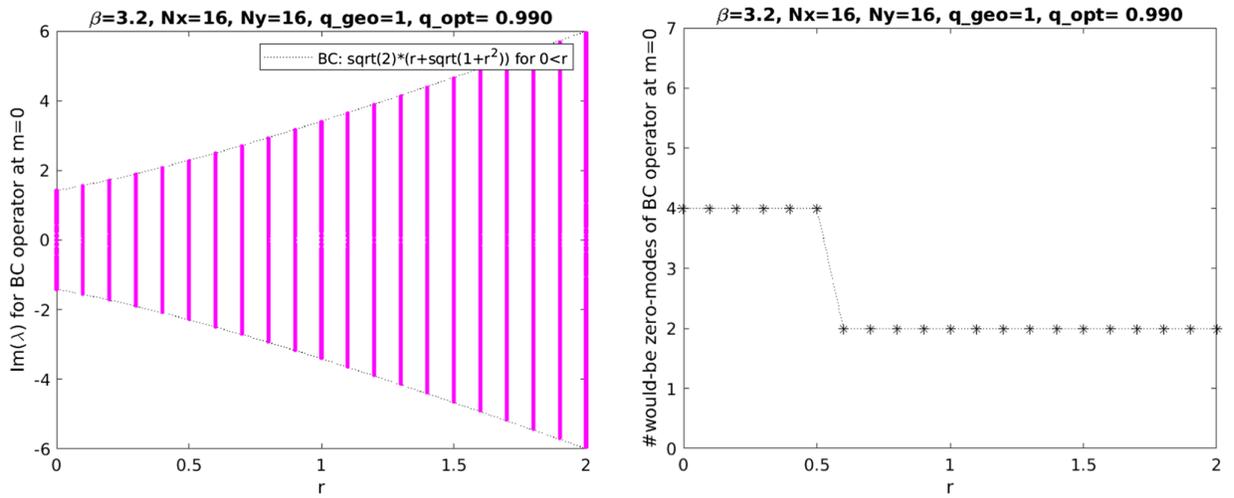

FIG. 21. Eigenvalues of the BC Dirac operator on an interacting background as a function of the species-lifting parameter r (left), and number of would-be zero modes versus r (right).
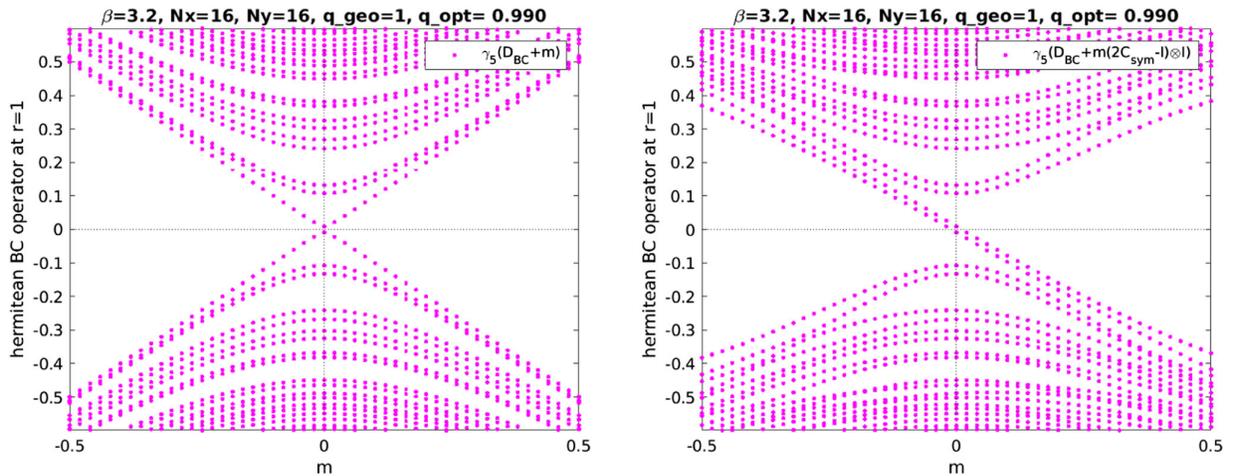

FIG. 22. Spectral flow of the BC Dirac operator, i.e., eigenvalues of $\gamma_5(D_{\text{BC}} + m)$ versus m (left), and eigenvalues of $\gamma_5(D_{\text{BC}} + m[2C_{\text{sym}} - 1] \otimes 1)$ versus m (right).
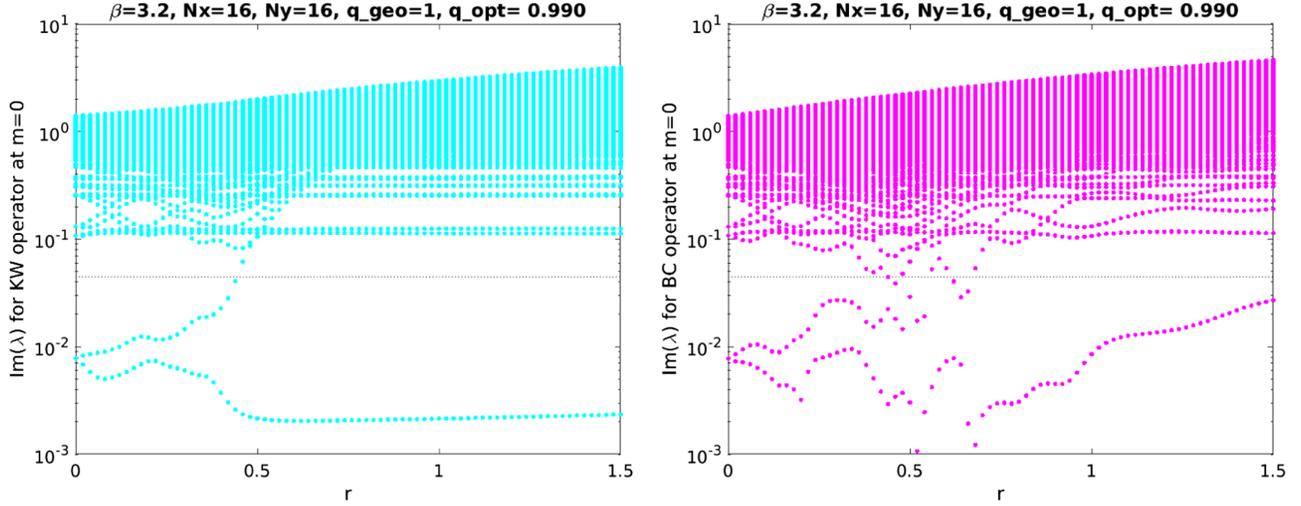
FIG. 23.   Upper half of the left panels of Figs. 18 and 21, but with logarithmic y-scale. The threshold for an eigenvalue to be considered a "would-be zero eigenvalue" is indicated by a dotted line.

KW case (Fig. 19) seems smaller, while in the BC case (Fig. 22) it seems comparable or larger. To corroborate this finding we display in Fig. 23 how the (positive) eigenvalues λ_{KW}/i and λ_{BC}/i evolve from the naive ones, as r grows from 0 to 1.5, this time with a logarithmic scale on the ordinate. The twofold degeneracy of the naive action is split for any $r > 0$, but the behavior of the (one) remaining would-be zero eigenvalue is different in the two panels. In the KW case it behaves very smoothly, and at $r \simeq 1$ it is *smaller* than in the naive or staggered case. On the other hand, in the BC case the would-be zero eigenvalue performs wild movements in the vicinity of the pole-merger zone at $r = 1/\sqrt{3}$ (see Ref. [8] for details), and at $r \simeq 1$ the deviation of the would-be zero eigenvalue from zero is *comparable in size* to the naive or staggered case. This raises further questions [58–62]; we shall briefly comment on this in Sec. IX.

VIII. KW AND BC FERMIONS WITH SPECIES-LIFTING TERMS

In Secs. III–VI, and VII we learned about the close relationship between a good chirality operator X which measures the chiralities $\langle \psi_i | X | \psi_i \rangle$ of the eigenmodes ψ_i of a given (doubled) D and the operator $D + r(1 \pm X \otimes \epsilon)$ or $D + r(1 \pm X \otimes \gamma_5)$ in which the tastes are separated[22] according to their chiralities. For KW fermions both $X = C_{\mathrm{sym}} \otimes \gamma_5$ and $X = [\frac{1}{2}(C_1 + C_2)^2 - 1] \otimes \gamma_5$ turned out to be good chirality operators, see footnote 20. For BC fermions both $X = [2C_{\mathrm{sym}} - 1] \otimes \gamma_5$ and $X = [\frac{1}{2}(C_1 +$

$C_2)^2 - 1] \otimes \gamma_5$ were found to be good chirality operators, see footnote 21. Hence the question arises whether one may add such an operator (without the factor γ_5) to separate the two species ("tastes") present in D_{KW} or D_{BC}.

In Fig. 24 the eigenvalues of the operators $D_{\mathrm{KW}} + s(1 - C_{\mathrm{sym}}) \otimes 1$ and $D_{\mathrm{KW}} + \frac{s}{2}(C_1 + C_2)^2 \otimes 1$ at $s = 1$ are shown (with $r = 1$ in D_{KW}). Both species-lifting terms work fine, but the curvature of the curved branches[23] agrees only in two of three cases with the curvature of the appropriate branch of the Wilson operator. The panels with the respective γ_5-chiralities show that in either branch there is exactly one mode[24] with chirality close to ± 1. This is different from the situation encountered in Sec. VI, where the chiralities of D_{KW} needed to be measured with $C_{\mathrm{sym}} \otimes \gamma_5$ or $\frac{1}{2}(C_1 + C_2)^2 \otimes \gamma_5$. But this difference is completely analogous to the difference between the D_{S} and D_{A} in Sec. III or the difference between D_{N} and D_{like} in Sec. IV.

In Fig. 25 the eigenvalues of the operators $D_{\mathrm{BC}} + s(1 - C_{\mathrm{sym}}) \otimes 1$ and $D_{\mathrm{BC}} + \frac{s}{2}(C_1 + C_2)^2 \otimes 1$ at $s = 1$ are shown (with $r = 1$ in D_{BC}). Both species-lifting terms work fine, but the curvature of the curved branches[25] agrees

---

[22]Starting from the staggered operator with $2^{d/2}$ species in d dimensions, the resulting Adams operator (7) has $2^{d/2-1}$ left-handed species in one branch and an equal number of right-handed species in the other branch. And starting from the naive operator with 2^d species, the resulting Adams-like operator (12) has 2^{d-1} left-handed species in one branch and an equal number of right-handed species in the other branch.

[23]For the operator $D_{\mathrm{KW}} + (1 - C_{\mathrm{sym}}) \otimes 1$ the eigenvalues in the left branch resemble the eigenvalues in the physical branch of D_{W}, and the right branch resembles the rightmost branch of $D_{\mathrm{W}} - 2$. On the other hand in $D_{\mathrm{KW}} + \frac{s}{2}(C_1 + C_2)^2 \otimes 1$ it takes $s = \frac{1}{2}$ to make the right branch mimic the rightmost branch of $D_{\mathrm{W}} - 3$.

[24]In the left panel of Fig. 24 the needle near $\lambda = 0$ points downwards, so everything is fine. In the right panel this needle points upwards, so consistency with the remainder of this article is lost. This could be avoided by using the operator $D_{\mathrm{KW}} + [2 - \frac{1}{2}(C_1 + C_2)^2] \otimes 1$ instead.

[25]The eigenvalues in the curved branch of $D_{\mathrm{BC}} + (1 - C_{\mathrm{sym}}) \otimes 1$ approximately coincide with the eigenvalues in the physical branch of D_{W}. On the other hand in $D_{\mathrm{BC}} + \frac{s}{2}(C_1 + C_2)^2 \otimes 1$ it takes $s = \frac{1}{2}$ to ensure that the eigenvalues in the right branch match those in the rightmost branch of $D_{\mathrm{W}} - 3$.
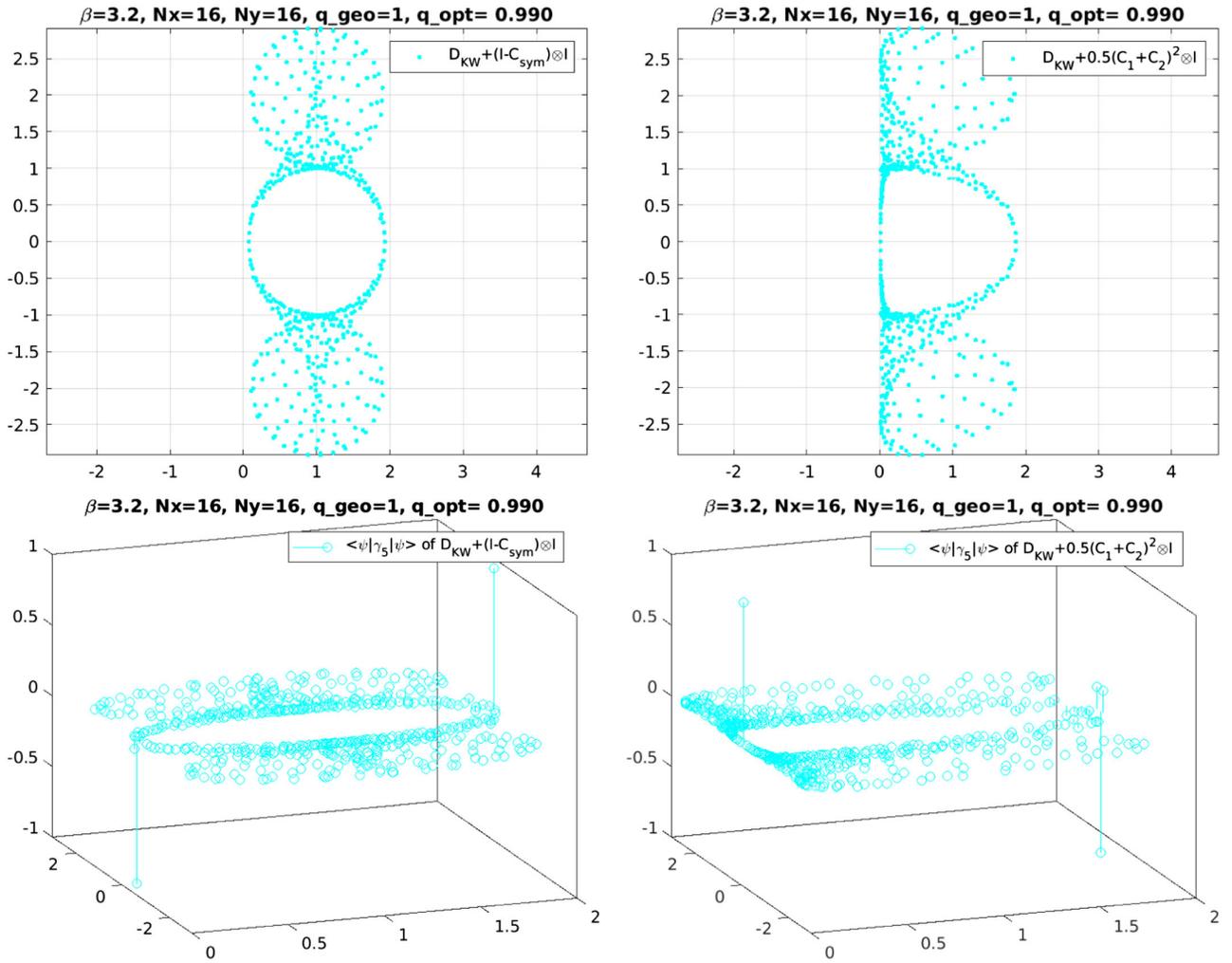
FIG. 24. Eigenvalues of D_{KW} with two lifting terms on a background with $q = 1$, and needle plots of the γ_5-chiralities in the pertinent left-right-eigenvector sandwiches.

only in one of two cases with the curvature of the appropriate branch of the Wilson operator. The panels with the respective γ_5-chiralities show that in either branch there is exactly one mode[26] with chirality close to ± 1. Again, either construction repeats the reasoning which led to the Adams operator (7) or the Adams-like operator (12).

In summary both D_{KW} and D_{BC} may be equipped with a species-lifting term. All four options discussed yield an undoubled fermion operator with additive mass renormalization. In the event $s(1 - C_{\mathrm{sym}}) \otimes 1$ is added, we recommend using $s = 1$. In the event $\frac{s}{2}(C_1 + C_2)^2 \otimes 1$ is added, we recommend using $s = \frac{1}{2}$, as this reduces unwanted mixings in the unphysical branch.

IX. CONCLUSIONS

Our goal was to provide evidence in the interacting theory that two minimally doubled fermion actions, namely

Karsten-Wilczek [1,2] and Borici-Creutz [3,4] fermions, perceive a global topological charge as foreseen in the seminal "anomaly" paper by Karsten and Smit [5].

In case of nonminimally doubled actions with (remnant exact) chiral symmetry, i.e., for staggered and naive fermions, it is known (perhaps not widely so) that special diligence is needed to select an appropriate chirality operator X to see the needles in the chirality plots $\langle \psi_i | X | \psi_i \rangle$ at position $\lambda_i \in \mathbb{C}$. In the case of Karsten-Wilczek fermions choosing X as $C_{\mathrm{sym}} \otimes \gamma_5$ or $\frac{1}{2}[(C_1 + C_2)^2 - 1] \otimes \gamma_5$ yields good results, and with Borici-Creutz fermions a similar statement holds true for X being $[2C_{\mathrm{sym}} - 1] \otimes \gamma_5$ or $\frac{1}{2}[(C_1 + C_2)^2 - 1] \otimes \gamma_5$.

We find that any appropriate choice of X for the needle plot would always yield the expected number of crossings in the spectral flow plot, and it would result in a useful definition of the topological charge via the "trace formula" discussed in Appendixes B and C.

To stress the universality of the underlying concept, we opted for showing similar plots with Wilson, Brillouin,

---

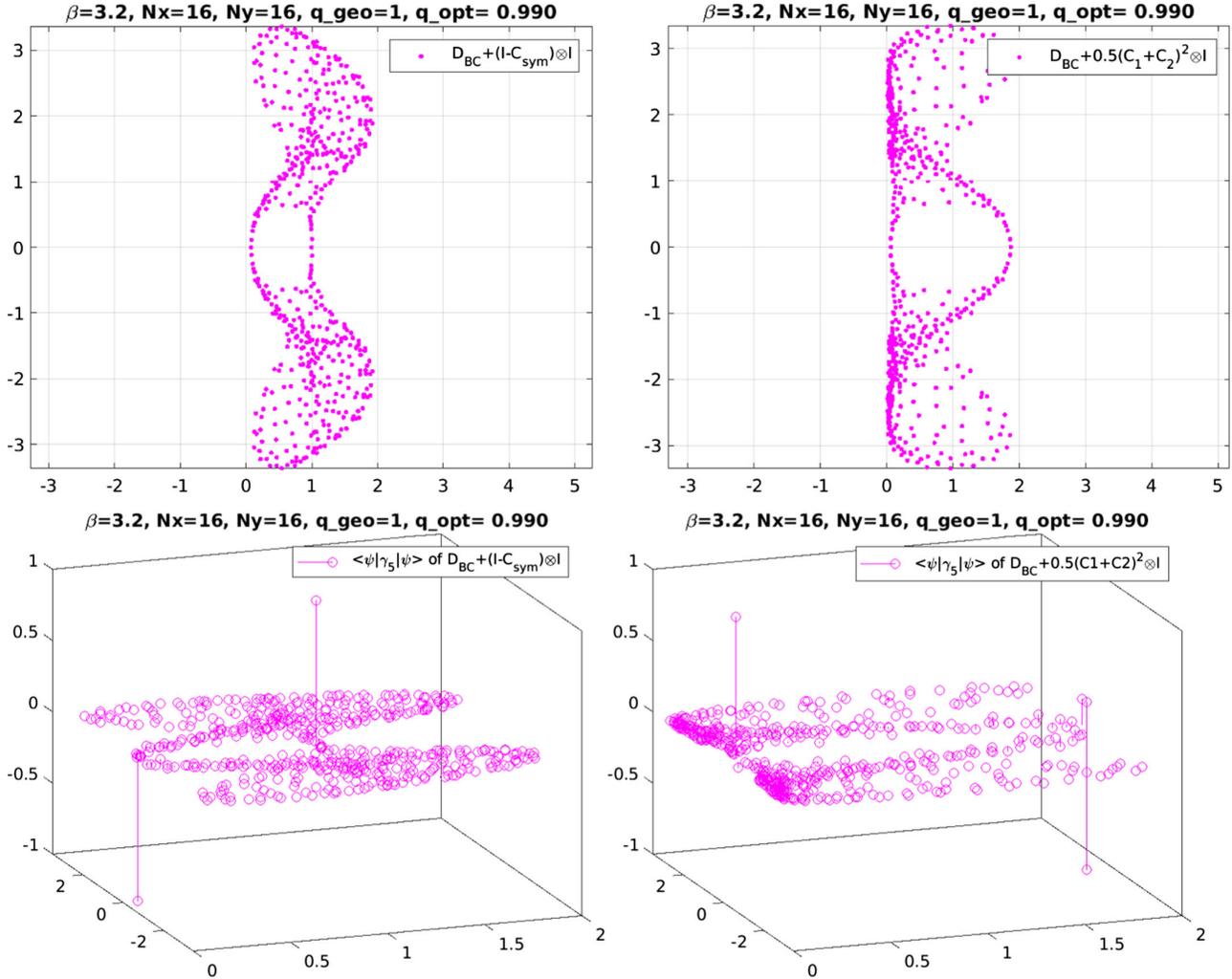[26]As to the signs of the needles footnote 24 applies again.

FIG. 25. Eigenvalues of D_{BC} with two lifting terms on a background with $q = 1$, and needle plots of the γ_5-chiralities in the pertinent left-right-eigenvector sandwiches.

staggered, Adams, naive and Adams-like fermions, plus two more varieties dubbed central-branch-squared and central-branch-squared-and-flipped fermions (of which the former one has very small additive mass shift). To limit the overall length, our numerics was restricted to 2D, but we plan to show similar plots in 4D at some point in the future.

An important part of the discussion focused on the intimate relation between a working chirality operator X for a given fermion action D and the lifting term that is needed to separate branches in D *according to their chirality* (typically $X \otimes \gamma_5$ or $X \otimes \epsilon$). This viewpoint emphasizes that Adams fermions are derived from staggered fermions in essentially the same way as the Adams-like action (12) is derived from the naive action (9). And it suggests dedicated splitting terms by means of which one of the species sitting in D_{KW} or D_{BC} can be lifted to become a doubler mode (albeit at the price of loosing the remnant chiral symmetry).

Finally the smallness of the (one) would-be zero eigenvalue of D_{KW} at $r = 1$ in Fig. 23 provides some (faint) evidence that the taste splitting for Karsten-Wilczek fermions might be smaller than for staggered fermions. Evidently nothing is known at this point about a potential change as a function of lattice spacing and box size, or whether it carries over to 4D and, finally, to spectroscopy. In the event this is not a fluke, this calls for further investigation.

APPENDIX A: NOTATION AND CLIFFORD ALGEBRA CONVENTIONS

Throughout this article ∂_μ and ∂_μ^* denote the discrete forward an backward derivative, respectively, and $\nabla_\mu = (\partial_\mu + \partial_\mu^*)/2$ is the symmetric derivative. These operators are gauged in the obvious manner; for instance the covariant symmetric derivative is

$$a\nabla_\mu\psi(x) = \frac{1}{2}[U_\mu(x)\psi(x+\hat{\mu}) - U_\mu^\dagger(x-\hat{\mu})\psi(x-\hat{\mu})], \quad (A1)$$

where $U_\mu(x)$ is the parallel transporter from $x + \hat{\mu}$ to x, and $\hat{\mu}$ denotes a times the unit vector in direction μ. Similarly, $\triangle_\mu = \partial_\mu^*\partial_\mu = \partial_\mu\partial_\mu^*$ denotes the second discrete derivative

$$a^2\triangle_\mu\psi(x) = U_\mu(x)\psi(x+\hat{\mu}) - 2\psi(x)$$
$$+ U_\mu^\dagger(x-\hat{\mu})\psi(x-\hat{\mu}), \quad (A2)$$

in the presence of a gauge field $U_\mu(x)$, and one defines $aD_\mu(x,y) = a\nabla_\mu(x,y)$ and

$$C_\mu(x,y) = \frac{1}{2}[U_\mu(x)\delta_{x+\hat{\mu},y} + U_\mu^\dagger(x-\hat{\mu})\delta_{x-\hat{\mu},y}]$$
$$= \frac{1}{2}a^2\triangle_\mu(x,y) + \delta_{x,y}. \quad (A3)$$

In d Euclidean spacetime dimensions (d even) it is customary to use a $2^{d/2}$-dimensional representation of the γ-matrices. In $d = 2$ dimensions we use $\gamma_1 = \sigma_1, \gamma_2 = \sigma_2$, along with

$$\gamma_5 = -i\gamma_1\gamma_2 = -i\sigma_1\sigma_2 = \sigma_3 = \text{diag}(+1,-1) \quad (A4)$$

and the matrices relevant to the Borici-Creutz discretization then take the form

$$\Gamma = \frac{1}{\sqrt{2}}(\sigma_1 + \sigma_2) = \frac{1}{\sqrt{2}}\begin{pmatrix} 0 & 1-i \\ 1+i & 0 \end{pmatrix}$$
$$= \begin{pmatrix} 0 & e^{-i\pi/4} \\ e^{+i\pi/4} & 0 \end{pmatrix}, \quad (A5)$$

$$\sigma_1' = \Gamma\sigma_1\Gamma = \frac{1}{2}(\sigma_1 + \sigma_2)\sigma_1(\sigma_1 + \sigma_2)$$
$$= \frac{1}{2}(\sigma_1 + \sigma_2 + \sigma_2 + \sigma_2\sigma_1\sigma_2) = \sigma_2, \quad (A6)$$

$$\sigma_2' = \Gamma\sigma_2\Gamma = \frac{1}{2}(\sigma_1 + \sigma_2)\sigma_2(\sigma_1 + \sigma_2)$$
$$= \frac{1}{2}(\sigma_1\sigma_2\sigma_1 + \sigma_1 + \sigma_1 + \sigma_2) = \sigma_1. \quad (A7)$$

Specifically for staggered and Adams fermions one defines the 1-hop operators

$$\Gamma_\mu(x,y) = \frac{1}{2}\eta_\mu(x)[U_\mu(x)\delta_{x+\hat{\mu},y} + U_\mu^\dagger(x-\hat{\mu})\delta_{x-\hat{\mu},y}]$$
$$= \eta_\mu(x)C_\mu(x), \quad (A8)$$

$$\Xi_\mu(x,y) = \frac{1}{2}\zeta_\mu(x)[U_\mu(x)\delta_{x+\hat{\mu},y} + U_\mu^\dagger(x-\hat{\mu})\delta_{x-\hat{\mu},y}]$$
$$= \zeta_\mu(x)C_\mu(x), \quad (A9)$$

with $\eta_\mu(x) = (-1)^{\sum_{\nu<\mu} x_\nu}$ and $\zeta_\mu(x) = (-1)^{\sum_{\nu>\mu} x_\nu}$. Based on this we define in $d = 2$ dimensions

$$\Gamma_5 \equiv \Gamma_{50} \equiv -\frac{i}{2}[\Gamma_1,\Gamma_2] = -\frac{i}{2}(\Gamma_1\Gamma_2 - \Gamma_2\Gamma_1), \quad (A10)$$

$$\Xi_5 \equiv \Gamma_{05} \equiv +\frac{i}{2}[\Xi_1,\Xi_2] = +\frac{i}{2}(\Xi_1\Xi_2 - \Xi_2\Xi_1), \quad (A11)$$

where the factor in front of (A10) is chosen to match the one in front of (A4). Evidently, in $d = 4$ dimensions $\Gamma_5 = \Gamma_5(x,y)$ and $\Xi_5 = \Xi_5(x,y)$ become 4-hop operators. Note that both Γ_5 and Ξ_5 are ϵ-Hermitian operators, as follows from (5), (6) along with $\Gamma_5 = \Gamma_5^\dagger$ and $\Xi_5 = \Xi_5^\dagger$.

In practice all the occurrences of $U_\mu(x)$ in this appendix (in ∇_μ, $\triangle_\mu$, C_μ, Γ_μ, Ξ_μ and thus in Γ_5 and Ξ_5) are replaced by the smeared gauge field $V_\mu(x)$, in our case via one stout step [28].

APPENDIX B: FERMIONIC TOPOLOGICAL CHARGES

In the continuum one finds the formula $q_{\text{fer}}[A] = (-1)^{d/2}\lim_{m\to 0} m \, \text{tr}(D_m^{-1}[A]\gamma_5)$ for the topological charge $q \in \mathbb{Z}$ of a gauge field $A_\mu(x)$. On the lattice similar formulas hold true, provided some diligence is applied to the "$\lim_{m\to 0}$ procedure" and the multiplicity is divided out [12,45]. In the following we use the sign for $d = 2$; it is straightforward to adjust this for $d = 4$.

In Fig. 26 we plot the behavior of the Wilson and Brillouin topological charges

$$q_{\text{W}}[U] = -m \, \text{tr}[(D_{\text{W}} + m)^{-1}I \otimes \gamma_5], \quad (B1)$$

$$q_{\text{B}}[U] = -m \, \text{tr}[(D_{\text{B}} + m)^{-1}I \otimes \gamma_5] \quad (B2)$$

as a function of m. Evidently, these charges are not integer valued, and it seems there is a pole structure in the vicinity of $m \simeq -0.1$, where the latter value coincides with the bare masses which would render $D_{\text{W}} + m$ or $D_{\text{B}} + m$ effectively massless, as seen in Figs. 1, 3.

Things become clearer upon considering a chirally improved version of the Wilson Dirac operator. Using $A_{\text{W}} \equiv (D_{\text{W}} - 1)^\dagger(D_{\text{W}} - 1)$, a chirally improved descendant at zero mass is defined via one KL11 iteration as $D_{\text{W}}^{\text{KL11}} = (D_{\text{W}} - 1)\frac{A_{\text{W}}+3}{3A_{\text{W}}+1} + 1$, and $D_{\text{B}}^{\text{KL11}}$ is defined similarly, see Ref. [35] for details. The eigenvalue spectra of
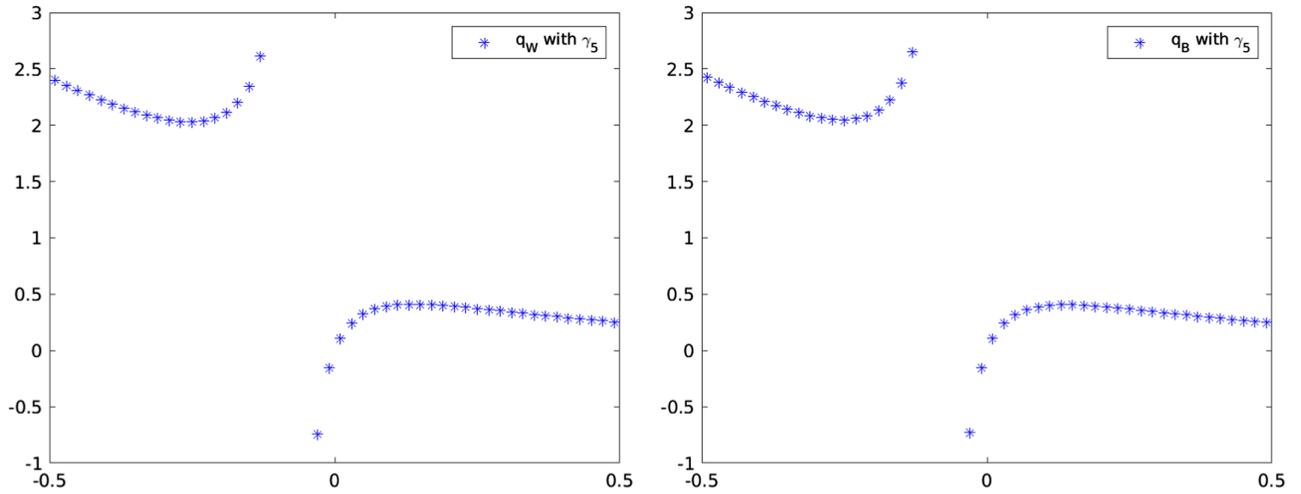
FIG. 26. Topological charge of the Wilson (left) and Brillouin (right) operator versus *am*.
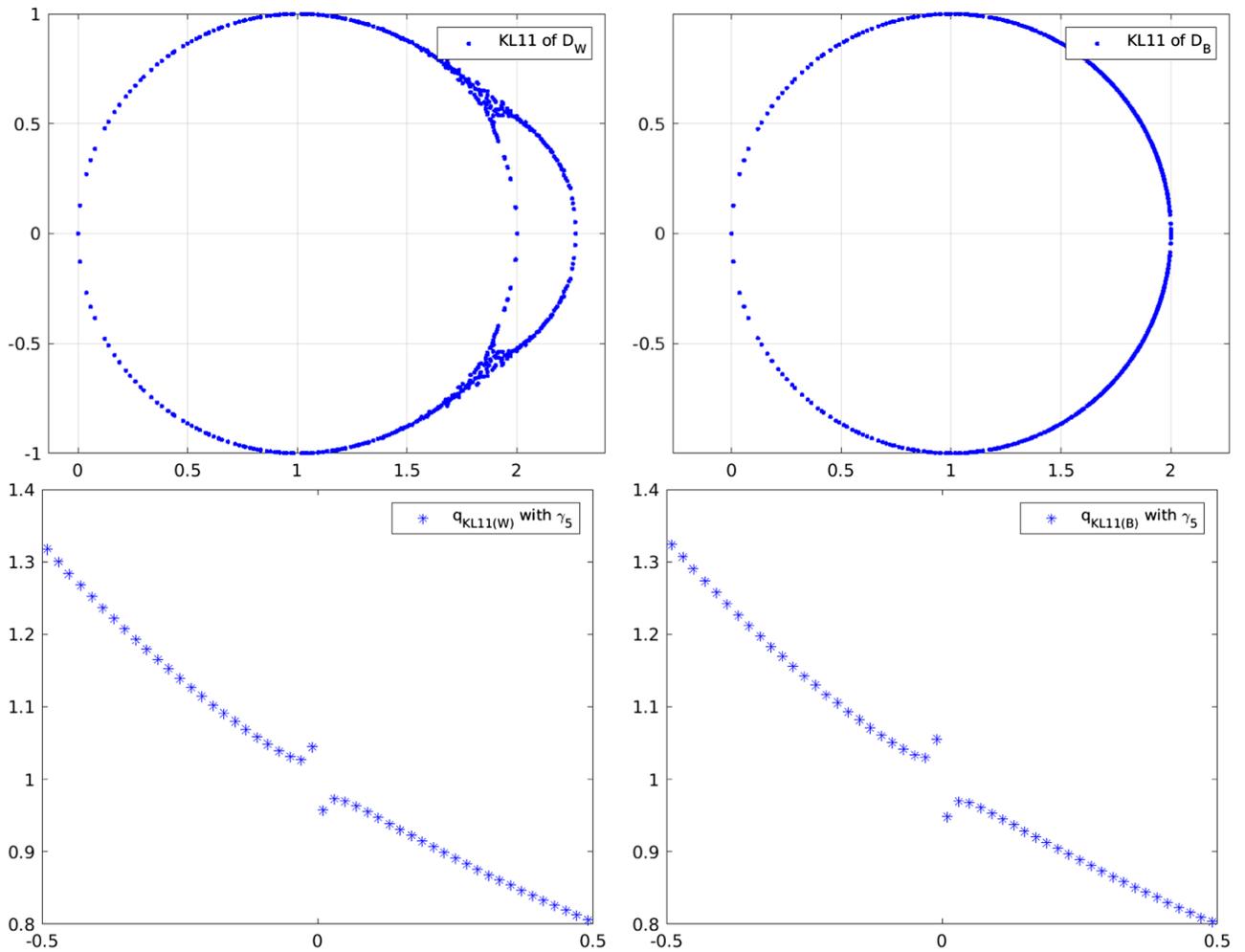
FIG. 27. Eigenvalues of the chirally improved Wilson and Brillouin operator (top), defined via one KL11 iteration (see text), along with their topological charges versus *am* (bottom).

these operators are shown in the top panels of Fig. 27. One notices that these operators show very small additive mass renormalization, and a few more Kenney-Laub steps make it zero within machine precision [35]. Upon plugging $D_{\mathrm{W}}^{\mathrm{KL11}}$ in place of D_{W} into (B1) and $D_{\mathrm{B}}^{\mathrm{KL11}}$ in place of D_{B} into (B2), one obtains the results in the bottom panels of
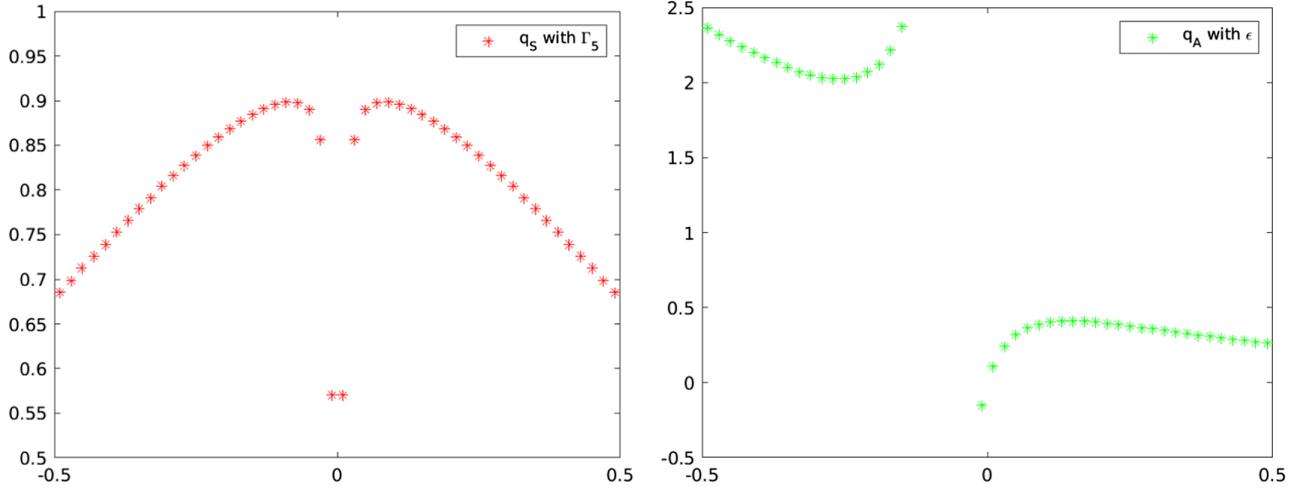
FIG. 28. Topological charge of the staggered (left) and Adams (right) operators versus am, using $\Gamma_5 = \Gamma_{50}$ as a chirally sensitive probe in the former case, and $\epsilon = \Gamma_{55}$ in the latter case.
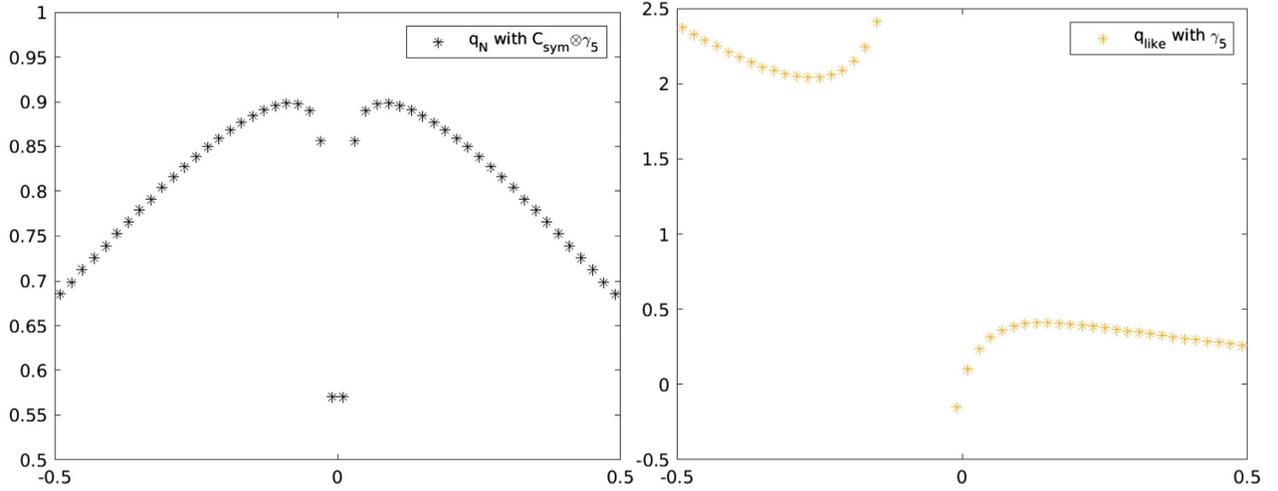

FIG. 29. Topological charge of the operator $D_N + m$ with $C_{sym} \otimes \gamma_5$ as a probe versus am (left), and of $D_{like} + m = D_N + 1 - C_{sym} + m$ with γ_5 as a probe versus am (right).

Fig. 27. This time it is clear that one should ignore a small "pole area" near $m = 0$, and read off the curve at a nearby m-value to find $q_W = 1$ and $q_B = 1$.

Given the arguments presented in Sec. III the staggered and Adams charges are

$$q_S[U] = -\frac{m}{2}\mathrm{tr}[(D_S + m)^{-1}\Gamma_{50}], \qquad (B3)$$

$$q_A[U] = -m\mathrm{tr}[(D_S + 1 - \Gamma_{05} + m)^{-1}\Gamma_{55}] \qquad (B4)$$

on a background U; they are shown as a function of m in Fig. 28. In the former case the function is even in m, in the latter case the behavior is similar to that of q_W and q_B. Again, one should ignore a pole area near $m = 0$, and read off the curve at a nearby m-value to find $q_S = 1$ and $q_A = 1$ (after some suitable interpolation and renormalization).

From the arguments presented in Sec. IV it follows that one should define the charges

$$q_N[U] = -\frac{m}{4}\mathrm{tr}[(D_N + m)^{-1}C_{sym} \otimes \gamma_5], \qquad (B5)$$

$$q_{like}[U] = -\frac{m}{2}\mathrm{tr}[(D_N + 1 - C_{sym} + m)^{-1}I \otimes \gamma_5] \qquad (B6)$$

for the naive and Adams-like operator, respectively. Their dependence on m is displayed in Fig. 29. Again, the former charge is even in m, the latter one is not.

Given the arguments presented in Sec. V it is clear that the natural definitions are

$$q_{cbs}[U] = +\frac{m}{2}\mathrm{tr}[(D_{cbs} + m)^{-1}I \otimes \gamma_5], \qquad (B7)$$
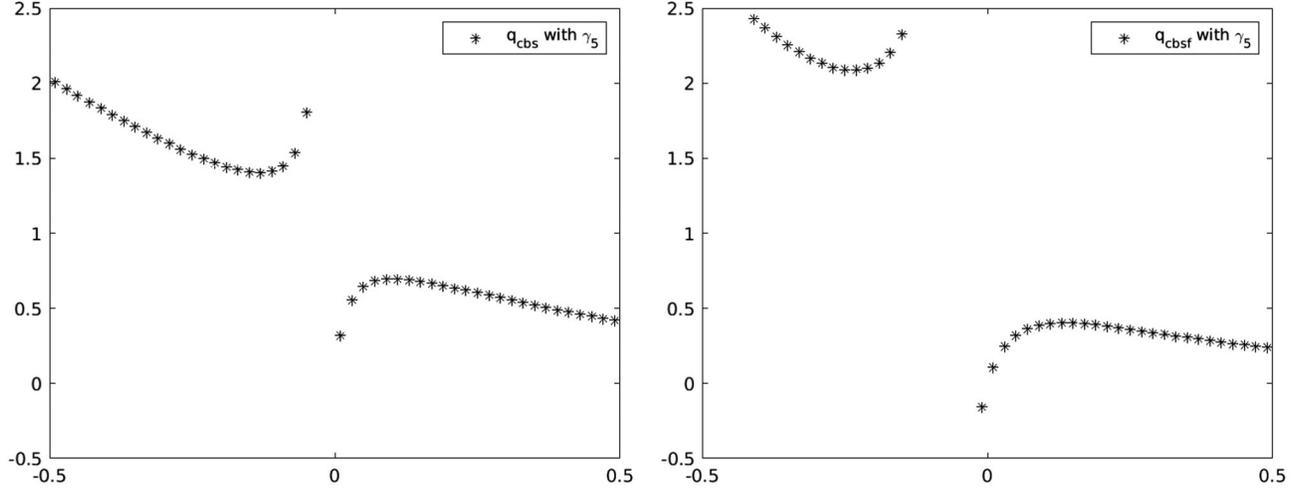
FIG. 30.　Topological charge of the central-branch-squared operator at $r = 1$ (left) and central-branch-squared-and-flipped operator at $r = \frac{1}{4}$ (right) versus am.
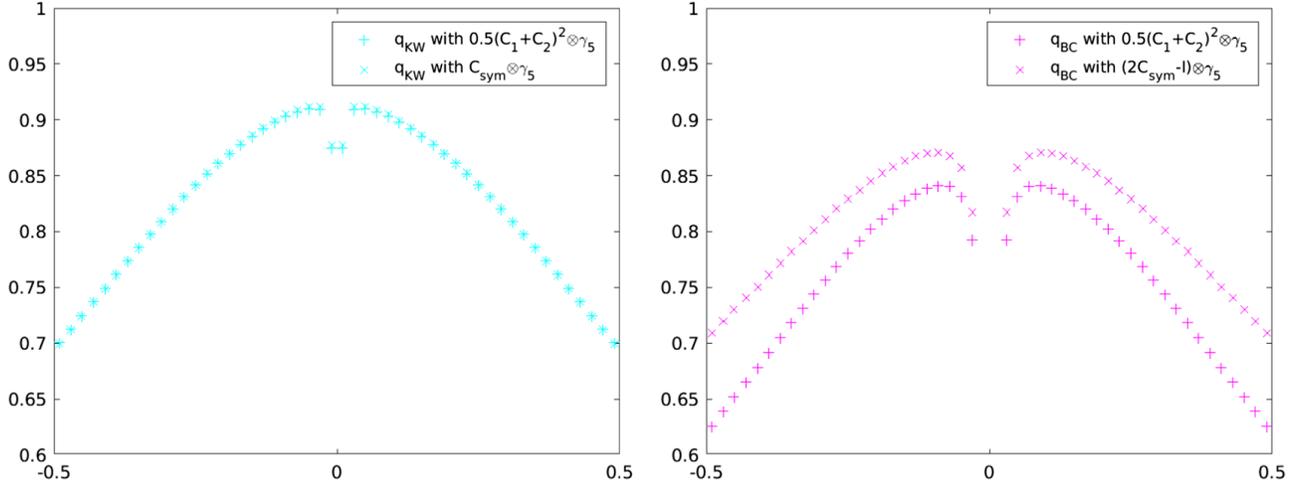

FIG. 31.　Topological charge of the KW (left) and BC (right) operator versus am. In either case a chirality operator based on $\frac{1}{2}(C_1 + C_2)^2$ and one based on C_{sym} are used.

$$q_{\text{cbsf}}[U] = -\frac{m}{2}\text{tr}[(D_{\text{cbsf}} + m)^{-1}I \otimes \gamma_5] \qquad (\text{B8})$$

for central-branch-squared and central-branch-squared-and-flipped fermions, respectively. The respective plots are found in Fig. 30, based on $r = 1$ in the former and $r = \frac{1}{4}$ in the latter case. The former formulation benefits from a rather small additive mass renormalization.

Finally, following the discussion in Secs. VI and VII, we define the charges

$$q_{\text{KW}}[U] = -\frac{m}{2}\text{tr}\left[(D_{\text{KW}} + m)^{-1}\frac{1}{2}(C_1 + C_2)^2 \otimes \gamma_5\right], \qquad (\text{B9})$$

$$q_{\text{KW}}[U] = -\frac{m}{2}\text{tr}\left[(D_{\text{KW}} + m)^{-1}C_{\text{sym}} \otimes \gamma_5\right], \qquad (\text{B10})$$

$$q_{\text{BC}}[U] = -\frac{m}{2}\text{tr}\left[(D_{\text{BC}} + m)^{-1}\frac{1}{2}(C_1 + C_2)^2 \otimes \gamma_5\right], \qquad (\text{B11})$$

$$q_{\text{BC}}[U] = -\frac{m}{2}\text{tr}\left[(D_{\text{BC}} + m)^{-1}[2C_{\text{sym}} - 1] \otimes \gamma_5\right] \qquad (\text{B12})$$

for Karsten-Wilczek and Borici-Creutz fermions, respectively. The four curves[27] are displayed in Fig. 31; they are even in m. For D_{KW} the two options of the charge operator work equally well, in line with what we reported in Sec. VI. For D_{BC} the chirality operator $[2C_{\text{sym}} - 1] \otimes \gamma_5$ seems to work marginally better than $\frac{1}{2}(C_1 + C_2)^2 \otimes \gamma_5$, again in line with Sec. VII.

In summary, a fermionic topological charge can be determined by reading off the m-dependent charge "slightly

---

[27]We checked that using $X = [\frac{1}{2}(C_1 + C_2)^2 - 1] \otimes \gamma_5$ instead of $X = \frac{1}{2}(C_1 + C_2)^2 \otimes \gamma_5$ brings no visible change in either panel of Fig. 31. This is in line with our statements regarding the needle plots (or diagonal part of the chirality operator) in Secs. VI and VII.

to the left" and "slightly to the right" of the polelike structure, and applying some suitable average (and possibly some renormalization and a cast-to-integer operation). The averaging procedure could be formalized, but it is clear that some arbitrariness remains. In practice all occurrences of $U_\mu(x)$ in this Appendix are replaced by the smeared gauge field $V_\mu(x)$. This holds for all Dirac matrices D and the staggered Γ_{50}, Γ_{05}, in line with Appendix A. Last but not least, in 4D the multiplicity factors need to be adjusted. In the staggered case it is $\frac{1}{4}$, in the Adams case $\frac{1}{2}$, the naive operator has $\frac{1}{16}$, and the Adams-like operator $\frac{1}{8}$. For D_{cbs} it is $\frac{1}{6}$, and for D_{cbsf} nothing changes.

APPENDIX C: ANALYTIC ARGUMENT

It is not surprising that the continuum formula $q_{\text{fer}}[A] = (-1)^{d/2}\lim_{m\to 0} m\,\text{tr}(D_m^{-1}[A]\gamma_5)$ has lattice counterparts as discussed in Appendix B. In the following we omit the factor $(-1)^{d/2}$ and concentrate on the Wilson operator D_{W}, but we see no obstacle to applying the argument to any other action. The argument is not entirely new [12,45], but it is still elucidating.

We want to feed the trace formula $q[U] = m\,\text{tr}(D_m^{-1}[U]\gamma_5)$ with the mode representation $D_m = \sum_i(\lambda_i + m)|\psi_i\rangle\langle\psi_i|$ of the Dirac operator, where $|\psi_i\rangle$ is the right eigenvector of D and $\langle\psi_i|$ is the left eigenvector (cf. footnote 3) on the gauge background U. In this representation the inverse is given by $D_m^{-1} = \sum_i(\lambda_i + m)^{-1}|\psi_i\rangle\langle\psi_i|$, thanks to the bi-orthogonality condition $\langle\psi_i|\psi_j\rangle = \delta_{ij}$. This yields $q = m\,\text{tr}(\sum_i(\lambda_i + m)^{-1}|\psi_i\rangle\langle\psi_i|\gamma_5) = m\sum_i(\lambda_i + m)^{-1}\,\text{tr}(|\psi_i\rangle\langle\psi_i|\gamma_5)$. Due to the cyclic property of the trace the last factor is $\text{tr}(\langle\psi_i|\gamma_5|\psi_i\rangle)$, and since the trace of a scalar object is just that object we have $q = m\sum_i(\lambda_i + m)^{-1}\langle\psi_i|\gamma_5|\psi_i\rangle$.

Next we should recall the needle plots for each action, for instance the right panel in Fig. 1 in case of D_{W}. Since $\langle\psi_i|\gamma_5|\psi_i\rangle \simeq 0$ for all i with $\text{Im}(\lambda_i)$ significantly nonzero, only the would-be zero modes in the physical branch and their siblings in the lifted branches contribute to this sum. But for these chiral modes $\langle\psi_i|\gamma_5|\psi_i\rangle \simeq \pm 1$, hence we have

$$q_{\text{lat}} = m\sum_{i\in\text{needles}}(\lambda_i + m)^{-1}\sigma_i, \qquad (\text{C1})$$

where σ_i is the sign of the needle associated with the exactly real mode i.

At this point we need to distinguish the various formulations and the dimensionality of spacetime. For instance for D_{W} in $d = 2$ dimensions we have three contributions

$$q_{\text{W}} = m\left\{\frac{1}{\lambda_0 + m} - \frac{2}{\lambda_{1-\text{lift}} + m} + \frac{1}{\lambda_{2-\text{lift}} + m}\right\} \qquad (\text{C2})$$

with alternating signs and weights reflecting the multiplicity of each branch. And for D_{W} in $d = 4$ dimensions the sign and weight sequence would be $\{+1, -4, +6, -4, +1\}$.

Next one should take into account that the two downward pointing needles in Fig. 1 are related by reflection symmetry. In fact the entire eigenvalue spectrum of the massless operator is symmetric about $\text{Re}(\lambda) = dr$, and for the massive operator this vertical reflection line is at $\text{Re}(\lambda) = dr + m$. Moreover, the eigenvalues in (C2) are exactly real, and the offset of λ_0 is basically given by the additive mass shift. Hence $\lambda_0 \simeq -m_{\text{crit}}$, where $m_{\text{crit}} < 0$ denotes the bare mass m at which D_{W} creates massless pions (on an infinite lattice). In consequence,

$$q_{\text{W}} = m\left\{\frac{1}{m - m_{\text{crit}}} - \frac{2}{2r + m} + \frac{1}{4r + m_{\text{crit}} + m}\right\}, \qquad (\text{C3})$$

where we take into account that $\lambda_{1-\text{lift}} = 2r$ for $m = 0$, modulo the "horizontal fuzziness" discussed in Sec. V. Bringing everything atop a common denominator yields

$$q_{\text{W}} = m\frac{(2r + m_{\text{crit}})^2 + (2r + m)^2}{(m - m_{\text{crit}})(2r + m)(4r + m_{\text{crit}} + m)} \qquad (\text{C4})$$

and for $m \simeq m_{\text{crit}}$ the latter expression simplifies to

$$q_{\text{W}} \simeq m\frac{2(2r + m_{\text{crit}})^2}{(m - m_{\text{crit}})(2r + m_{\text{crit}})(4r + 2m_{\text{crit}})}$$
$$= \frac{m}{m - m_{\text{crit}}}, \qquad (\text{C5})$$

which underpins the pole structure that shows up near $m_{\text{crit}} < 0$ in the right panel of Fig. 26. In fact, for the chirally improved Wilson operator $D_{\text{W}}^{\text{KL11}}$ the lower left panel in Fig. 27 demonstrates that its additive mass shift is much smaller than that of the Wilson operator.

For doubled chiral actions the basic formula (C1) still holds true, but the sum is dominated by the would-be zero modes which come in complex conjugate pairs. Here it is important that the σ_i reflect the chiralities as determined by an appropriate chirality operator. For instance, for staggered fermions σ_i refers to Γ_5 so that the pairs have *like sign* (with ϵ they would have opposite sign and thus cancel). Specifically in $d = 2$ dimensions one has

$$q_{\text{S}} = \frac{m}{2}\left\{\frac{1}{+i\epsilon + m} + \frac{1}{-i\epsilon + m}\right\}$$
$$= \frac{m}{2}\frac{2m}{(i\epsilon + m)(-i\epsilon + m)} = \frac{m^2}{\epsilon^2 + m^2}, \qquad (\text{C6})$$

which suggests that there is a double-pole structure near $m = 0$. In $d = 4$ dimensions the factor in front is $\frac{m}{4}$ and

there are $4|q|$ contributions, so the conclusion is unchanged. Similarly, the argument goes through for KW and BC fermions.

Looking at the plots assembled in Appendix B we find the prediction of the pole structure confirmed, both for nonchiral and chiral (doubled) actions. However, it is clear that the curves include a significant regular part which is not covered by the argument. Regarding the nonchiral actions we comment that mapping out the pole structure in (C5) provides a handle at λ_0 (on a given configuration) and thus at the additive mass shift $-m_{\text{crit}}$ (after averaging over configurations). This approach does not require any eigenvalue and/or eigenvector computation, nor does it involve spectroscopy, but we do not know whether it is very practical.

[1] L. H. Karsten, Phys. Lett. **104B**, 315 (1981).
[2] F. Wilczek, Phys. Rev. Lett. **59**, 2397 (1987).
[3] M. Creutz, J. High Energy Phys. 04 (2008) 017.
[4] A. Borici, Phys. Rev. D **78**, 074504 (2008).
[5] L. H. Karsten and J. Smit, Nucl. Phys. **B183**, 103 (1981).
[6] H. B. Nielsen and M. Ninomiya, Nucl. Phys. **B185**, 20 (1981); **B195**, 541(E) (1982).
[7] H. B. Nielsen and M. Ninomiya, Nucl. Phys. **B193**, 173 (1981).
[8] S. Durr and J. H. Weber, Phys. Rev. D **102**, 014516 (2020).
[9] H. S. Sharatchandra, H. J. Thun, and P. Weisz, Nucl. Phys. **B192**, 205 (1981).
[10] H. Kluberg-Stern, A. Morel, O. Napoly, and B. Petersson, Nucl. Phys. **B220**, 447 (1983).
[11] M. F. L. Golterman and J. Smit, Nucl. Phys. **B245**, 61 (1984).
[12] J. Smit and J. C. Vink, Nucl. Phys. **B286**, 485 (1987).
[13] T. Blum, C. DeTar, S. Gottlieb, K. Rummukainen, U. M. Heller, J. E. Hetrick, D. Toussaint, R. L. Sugar, and M. Wingate, Phys. Rev. D **55**, R1133 (1997).
[14] K. Orginos and D. Toussaint (MILC Collaboration), Phys. Rev. D **59**, 014501 (1998).
[15] W. J. Lee and S. R. Sharpe, Phys. Rev. D **60**, 114503 (1999).
[16] F. Knechtli and A. Hasenfratz, Phys. Rev. D **63**, 114502 (2001).
[17] M. Pernici, Phys. Lett. B **346**, 99 (1995).
[18] B. C. Tiburzi, Phys. Rev. D **82**, 034511 (2010).
[19] M. Creutz, T. Kimura, and T. Misumi, J. High Energy Phys. 12 (2010) 041.
[20] J. S. Schwinger, Phys. Rev. **128**, 2425 (1962).
[21] J. H. Lowenstein and J. A. Swieca, Ann. Phys. (N.Y.) **68**, 172 (1971).
[22] M. M. Ansourian, Phys. Lett. **70B**, 301 (1977).
[23] H. Dilger, Phys. Lett. B **294**, 263 (1992).
[24] H. Dilger, Int. J. Mod. Phys. C **06**, 123 (1995).
[25] S. Durr, Phys. Rev. D **85**, 114503 (2012).
[26] D. Albandea, P. Hernández, A. Ramos, and F. Romero-López, Eur. Phys. J. C **81**, 873 (2021).
[27] T. Eichhorn and C. Hoelbling, arXiv:2112.05188.
[28] C. Morningstar and M. J. Peardon, Phys. Rev. D **69**, 054501 (2004).
[29] S. Durr and J. H. Weber, arXiv:2108.11766.
[30] K. G. Wilson, Phys. Rev. D **10**, 2445 (1974).

[31] I. Montvay and G. Münster, *Quantum Fields on a Lattice* (Cambridge University Press, Cambridge, UK, 1994).
[32] I. Hip, T. Lippert, H. Neff, K. Schilling, and W. Schroers, Nucl. Phys. B, Proc. Suppl. **106**, 1004 (2002).
[33] R. G. Edwards, U. M. Heller, and R. Narayanan, Nucl. Phys. **B522**, 285 (1998).
[34] S. Durr and G. Koutsou, Phys. Rev. D **83**, 114512 (2011).
[35] S. Durr and G. Koutsou, arXiv:1701.00726.
[36] W. Bietenholz and I. Hip, Nucl. Phys. **B570**, 423 (2000).
[37] W. Bietenholz and S. Shcheredin, Nucl. Phys. **B754**, 17 (2006).
[38] C. Gattringer, C. Hagen, C. B. Lang, M. Limmer, D. Mohler, and A. Schafer, Phys. Rev. D **79**, 054501 (2009).
[39] C. Gattringer *et al.* (BGR and Bern-Graz-Regensburg Collaborations), Nucl. Phys. **B677**, 3 (2004).
[40] L. Susskind, Phys. Rev. D **16**, 3031 (1977).
[41] N. Kawamoto and J. Smit, Nucl. Phys. **B192**, 100 (1981).
[42] E. Follana, A. Hart, and C. T. H. Davies (HPQCD and UKQCD Collaborations), Phys. Rev. Lett. **93**, 241601 (2004).
[43] S. Durr, C. Hoelbling, and U. Wenger, Phys. Rev. D **70**, 094502 (2004).
[44] J. Smit and J. C. Vink, Phys. Lett. B **194**, 433 (1987).
[45] J. Smit and J. C. Vink, Nucl. Phys. **B303**, 36 (1988).
[46] M. L. Laursen, J. Smit, and J. C. Vink, Nucl. Phys. **B343**, 522 (1990).
[47] S. J. Hands and M. Teper, Nucl. Phys. **B347**, 819 (1990).
[48] D. H. Adams, Phys. Rev. Lett. **104**, 141602 (2010).
[49] V. Azcoiti, G. Di Carlo, E. Follana, and A. Vaquero, Phys. Lett. B **744**, 303 (2015).
[50] D. H. Adams, Phys. Lett. B **699**, 394 (2011).
[51] C. Hoelbling, Phys. Lett. B **696**, 422 (2011).
[52] P. de Forcrand, A. Kurkela, and M. Panero, J. High Energy Phys. 04 (2012) 142.
[53] S. Durr, Phys. Rev. D **87**, 114501 (2013).
[54] A. Chowdhury, A. Harindranath, J. Maiti, and S. Mondal, J. High Energy Phys. 02 (2013) 037.
[55] T. Misumi and Y. Tanizaki, Prog. Theor. Exp. Phys. **2020**, 033B03 (2020).
[56] T. Misumi and J. Yumoto, Phys. Rev. D **102**, 034516 (2020).
[57] J. Yumoto and T. Misumi, J. High Energy Phys. 02 (2022) 104.

[58] P. F. Bedaque, M. I. Buchoff, B. C. Tiburzi, and A. Walker-Loud, Phys. Lett. B **662**, 449 (2008).

[59] T. Kimura, S. Komatsu, T. Misumi, T. Noumi, S. Torii, and S. Aoki, J. High Energy Phys. 01 (2012) 048.

[60] T. Misumi, J. High Energy Phys. 08 (2012) 068.

[61] T. Misumi, T. Kimura, and A. Ohnishi, Phys. Rev. D **86**, 094505 (2012).

[62] J. H. Weber, Proc. Sci., LATTICE2016 (**2017**) 250 [arXiv:1611.08388].